5C

BNWL-1703
UC-11

13-1

Variable Thickness Transient Groundwater Flow Model Theory and Numerical Implementation

by
K. L. Kipp
A. E. Reisenauer
C. R. Cole
C. A. Bryan

1972
(Updated 1976)

This report is based on work sponsored by the Atlantic Richfield Hanford Company under Energy Research and Development Administration Contract AT(45-l)-2130

Battelle
Pacific Northwest Laboratories

BNWL-1703

NOTICE

PACIFIC NORTHWEST LABORATORY
operated by
BATTELLE
for the
ENERGY RESEARCH AND DEVELOPMENT ADMINISTRATION
Under Contract E(45-1)-1830

Printed in the United States of America
Available from
National Technical Information Service
U.S. Department of Commerce
5285 Port Royal Road
Springfield, Virginia 22151
Price: Printed Copy $5.50; Microfiche $2.25

BNWL-1703
UC-11

Variable Thickness Transient Groundwater Flow Model Theory and Numerical Implementation

by
K. L. Kipp
A. E. Reisenauer
C. R. Cole
C. A. Bryan

1972
(Updated 1976)

This report is based on work sponsored by the Atlantic Richfield Hanford Company under Energy Research and Development Administration Contract AT(45-l)-2130

Battelle
Pacific Northwest Laboratories

BNWL-1703

NOTICE

PACIFIC NORTHWEST LABORATORY
operated by
BATTELLE
for the
ENERGY RESEARCH AND DEVELOPMENT ADMINISTRATION
Under Contract E(45-1)-1830

Printed in the United States of America
Available from
National Technical Information Service
U.S. Department of Commerce
5285 Port Royal Road
Springfield, Virginia 22151
Price: Printed Copy $5.50; Microfiche $2.25

BNWL-1703

VARIABLE THICKNESS TRANSIENT GROUNDWATER FLOW MODEL THEORY AND NUMERICAL IMPLEMENTATION

By

K. L. Kipp**
A. E. Reisenauer
C. R. Cole
C. A. Bryan*

Water and Land Resources Department
*University of Montana, Missoula, Montana
**AERE Harwell, Oxfordshire, England

1972
(Updated 1976)

This report is based on work sponsored by the Atlantic Richfield Hanford Company under United States Energy Research and Development Administration Contract AT(45-1)-2130

BATTELLE
PACIFIC NORTHWEST LABORATORIES
RICHLAND, WASHINGTON 99352

SUMMARY

Modeling of radionuclide movement in the groundwater system beneath the Hanford Reservation requires mathematical simulation of the two-dimensional flow in the unconfined aquifer. This was accomplished using the nonlinear, transient Boussinesq equation with appropriate initial and boundary conditions, including measured Columbia River stages and rates of wastewater disposal to the ground. The heterogeneous permeability (hydraulic conductivity) distribution was derived by solution of the Boussinesq equation along instantaneous streamtubes of flow employing a measured water table surface and a limited number of field-measured hydraulic conductivity values. Use of a successive line over-relaxation technique with unequal time steps resulted in a more rapid convergence of the numerical solution than with previous techniques. The model was used to simulate the water table changes for the period 1968 through 1973 using known inputs and boundary conditions. A comparison of calculated and measured water table elevations was made at specific well locations and the quality of the verification simulation was evaluated using a data retrieval and display system. Agreement between the model results and measured data was good over two-thirds of the Hanford Reservation. The capability of the model to simulate flow with time-varying boundary conditions, complex boundary shapes and a heterogeneous distribution of aquifer properties was demonstrated.

CONTENTS

FIGURES

SYMBOLS AND DIMENSIONS

h	hydraulic potential, ft
q	infiltration flux, $(ft^3/day)/ft^2$
R	region of the flow system
$r_{i,j}$	elemental square within region R at index i,j
t	time variable, days
K	hydraulic conductivity, ft/day
x,y,z	Cartesian coordinate system, ft
Γ	boundary of $r_{i,j}$ at node i,j
δ_i	steady term in the transmissivity calculation at step i
Δ_i	transient term in the transmissivity calculation at step i
σ	storage coefficient,(dimensionless)
ρ	density of water, lbs/ft^3
$\underline{\nabla}$	gradient operator
$\underline{\underline{A}}$	a matrix

SYMPOLS AND DIMENSIONS (continued)

$\underline{b}$	a vector
H	water boundary potential, ft
h_{ij}^{n}	discretized potential at time plane n, node i,j, ft
h_{ij}^{o}	aquifer bottom surface at node i,j, ft
n	outward vector normal to surface
p	pressure, lb/ft^2
$\underline{q}$	Darcy velocity, ft/day
q'	infiltration or accretion flux, $(ft^3/day)/ft^2$
Q_{ij}	volumetric infiltration flow rate at node i,j, ft^3/day
$\underline{V}$	pore velocity, ft/day
ω	relaxation factor
γ	specific weight of water, lb/ft^3
ϕ	potential function for Darcy flow, ft^2/day
η	free surface position, ft
Δx	nodal spacing, ft

VARIABLE THICKNESS TRANSIENT GROUNDWATER FLOW MODEL THEORY AND NUMERICAL IMPLEMENTATION*

INTRODUCTION

The saturated groundwater flow model for the unconfined aquifer described in this report was developed as part of the Radionuclides in Soils program, a study of the potential movement of radionuclides in the hydrogeologic system of the Hanford Reservation. The output of this model is the transient groundwater flow potential distribution for the area simulated from which seepage velocities can readily be computed.

This report contains the 1) mathematical model and its assumptions, 2) numerical formulation of the equations, 3) acquisition and preparation of the boundary and initial conditions and source terms, 4) numerical solution techniques used in obtaining solutions or simulations of the flow field, and 5) results of the verification simulation of a 6-year period. A separate document, BNWL-1706, The Transmissivity Iterative Calculation Routine - Theory and Numerical Implementation, covers the derivation and preparation of the aquifer property values: hydraulic conductivity and storage coefficient.

FORMULATION OF THE MATHEMATICAL VARIABLE THICKNESS TRANSIENT MODEL

The Variable Thickness Transient (VTT) Model was developed using the Boussinesq equation with appropriate initial and boundary conditions. This equation is derived by vertically averaging the three-dimensional equation governing incompressible, Darcian groundwater flow. Thus the independent spatial variables are in the horizontal plane and the nonlinear, free-surface boundary condition is incorporated into the governing differential equation. Furthermore, in addition to that flow derived from the storage coefficient, any flux resulting from vertical infiltration from the partially saturated zone above the free surface appears as a source term in the Boussinesq equation. All aquifer properties are represented by their average value over the vertical thickness of saturated flow. A significant capability of this numerical formulation of the mathematical model is its ability to handle heterogeneous distributions of hydraulic conductivity and storage coefficient.

*This document has been reveiwed by Atlantic Richfield Hanford Company and authorized for publication by the Manager, Groundwater Management.

Appropriate boundary conditions include impermeable boundaries through which no flow occurs and known potential boundaries where an open body of water joins directly to the aquifer.

The model simulates the flow of an incompressible fluid that saturates a rigid, porous soil matrix. Compressibility effects of the fluid and matrix can safely be neglected under conditions of unconfined or free-surface flow.

The hydraulic conductivity (K) is assumed to be isotropic but heterogeneous. Darcy's law is presumed to govern the flow.

$$\underline{q} = -K\underline{\nabla}\phi \tag{1}$$

where $\phi = \frac{p}{\gamma} + z$.

Applying continuity considerations for incompressible flow leads to

$$\underline{\nabla} \cdot (K\underline{\nabla}\phi) = 0 \tag{2}$$

whose solutions are potentials of the Poisson type. For heterogeneous, isotropic media with negligible soil and water compressibilities, the above equation becomes:

$$K\nabla^2\phi + \underline{\nabla}K \cdot \underline{\nabla}\phi = 0. \tag{3}$$

Boundary Conditions

1) Where the aquifer contacts a body of free water, the boundary is a surface along which the potential ϕ is known. In the general transient case with the water surface sloping in the direction of flow, such as along a river,

$$\phi = H(\underline{r},t) \tag{4}$$

where $\underline{r}$ locates a point on the boundary. This boundary is not an equipotential surface and $\underline{\nabla}\phi$ is not necessarily normal to it.

2) An impermeable boundary has no flow across it and is usually fixed in space. Thus,

$$\frac{\partial\phi}{\partial n} = 0 \tag{5}$$

along an impermeable boundary where n designates the outward normal to the boundary.

3) A free surface is a boundary whose location in space and time is unknown before the problem is solved. By neglecting capillary effects, it becomes a sharp interface. Therefore, two boundary conditions need to be imposed. Flow in the capillary fringe is neglected. Let $z = \eta(x,y,t)$ designate the free surface. Since atmospheric pressure over the free surface is taken to be zero, the defining equation for ϕ becomes

$$\phi - z = 0. \tag{6}$$

The kinematic boundary condition comes from the fact that a particle initially on the free surface remains on it as the surface moves. Mathematically this means that the substantial derivative (or the derivative following the motion) of the equation defining the free surface must equal zero.[1] Thus,

$$\frac{D}{Dt}(\phi - z) = \left[\frac{\partial}{\partial t} + (\underline{V} \cdot \underline{\nabla})\right](\phi - z) = 0 \tag{7}$$

where $\underline{V} = \frac{\underline{q}}{\sigma} = \frac{-K\underline{\nabla}\phi}{\sigma}$.

Substituting for the velocities gives the nonlinear, kinematic, free surface boundary condition:

$$\frac{\sigma}{K}\frac{\partial \phi}{\partial t} - (\underline{\nabla}\phi)^2 + \frac{\partial \phi}{\partial z} = 0 \quad \text{on} \quad z = \eta. \tag{8}$$

A free surface with accretion occurs when there is an infiltration flux across that surface.

$$\sigma\frac{\partial \phi}{\partial t} - K(\underline{\nabla}\phi)^2 + \frac{\partial \phi}{\partial z}(K + q') - q' = 0. \tag{9}$$

Equation 9 is the result of modifying Equation 8 to include the rate of accretion or infiltration q', [units $(L^3/T/L^2)$ referenced to a horizontal surface z = constant.

4) A surface of seepage is a stationary surface, fixed in space, along which pressure is atmospheric ($p = 0$); here the water leaves the porous medium and enters free space outside the aquifer. Thus,

$$\phi = z.$$

Initial Condition

The initial distribution of the dependent variable $\phi(r,t)$ must be known at time zero.

The derivations of the above differential equation and boundary conditions can be found in a basic groundwater flow reference such as Bear, et al.,[2] or Polubarinova-Kochina.[3] Obtaining a solution to the free surface boundary condition (Equation 9 above) for the general case is difficult primarily because of its nonlinear characteristic. Furthermore, the knowledge of the three-dimensional potential distribution and three-dimensional distribution of aquifer properties is usually insufficient. Therefore, an approximate method has been adopted which facilitates the mathematical treatment of the groundwater flow problem.

THE DUPUIT - BOUSSINESQ APPROXIMATION

The Dupuit or hydraulic theory of groundwater flow rests on the assumptions that the free surface has only small inclinations and the slope of the aquifer bottom is slight. Thus, the streamlines are essentially horizontal. As a result, vertical velocities can be neglected so that the equations of flow can be averaged in the vertical direction. Surfaces of seepage are not considered in this theory. Flow rates are exact but the free surface profile is in error, especially in areas of large curvature.[4] The result of averaging Equation 2 in the vertical direction from the aquifer bottom, h^o, to the free surface, h, and including the free surface boundary conditions on Equation 2 results in

$$\underline{\nabla} \cdot K(h - h^o)\underline{\nabla}h = \sigma\frac{\partial h}{\partial t} - q' \qquad (11)$$

where $q' > 0$ is infiltration, the potential head $\phi(x,y,z,t)$ is replaced by the elevation of the free surface, $h(x,y,t)$, and $\underline{\nabla}$ is the two-dimensional (x,y) gradient operator.

Equation 11 is known as the Boussinesq[5] equation of unsteady flow.* The number of spatial dimensions has been reduced from 3 to 2 and all of the aquifer properties are represented by their average over the saturated thickness of the aquifer. The nonlinear free surface boundary condition has made the differential equation nonlinear, but the unknown surface configuration is now identical to the unknown dependent variable.

Boundary and Initial Conditions for the Boussinesq Equation

1) Water boundaries are approximated by vertical surfaces that must completely penetrate the entire saturated thickness of the aquifer. Along them the hydraulic potential is specified as

$$h = H(x,y,t) \qquad (12)$$

*Development of this equation is expanded in Appendix D.

2) Impermeable boundaries are also approximated as vertical surfaces through which no flow occurs:

$$\frac{\partial h}{\partial n} = 0 \qquad (13)$$

3) Accretion caused by infiltration from above or seepage from below has been imbedded into the differential equation itself as the term q' in Equation 11.

Infiltration across the lateral boundaries of the region is sometimes given as a specified flux across such vertical boundary surfaces. In this case, the boundary condition takes the form

$$\underline{q} \cdot \hat{n} = -K(h - h^{o}) \frac{\partial h}{\partial n}$$

where $\hat{n}$ denotes the outward normal to the boundary and $\underline{q} \cdot \hat{n} < 0$ means flow into the region. This condition is generally used in modeling an open aquifer region when some value of the flow from regions outside the simulated portion is assumed.

The free surface boundary condition with accretion is also incorporated into the differential equation. Surfaces of seepage had to be neglected in order to carry out the averaging in the vertical direction. Figure 1 shows a typical portion of an aquifer with the boundary conditions illustrated. For application of the model to the Hanford unconfined aquifer, flow through the bottom boundary was assumed to be negligible.

The initial potentials at each node, h_{ij} are the groundwater levels obtained from interpolation between measurements. In parctice the groundwater levels are measured at selected well sites from which a contour map is prepared. The values of h_{ij} are obtained from the contour map.

In order to use the above set of equations to simulate groundwater flow, information is needed to: 1) locate the impermeable and water boundary surfaces in the horizontal coordinate system of the problem; 2) specify the time variation of the potential along the water boundaries; 3) determine infiltration flux distribution over the flow region; 4) derive the horizontal distribution of the heterogeneous hydraulic conductivity and storage coefficient; 5) specify the initial potential distribution at time, t; and 6) locate the surface that represents the impermeable aquifer bottom.

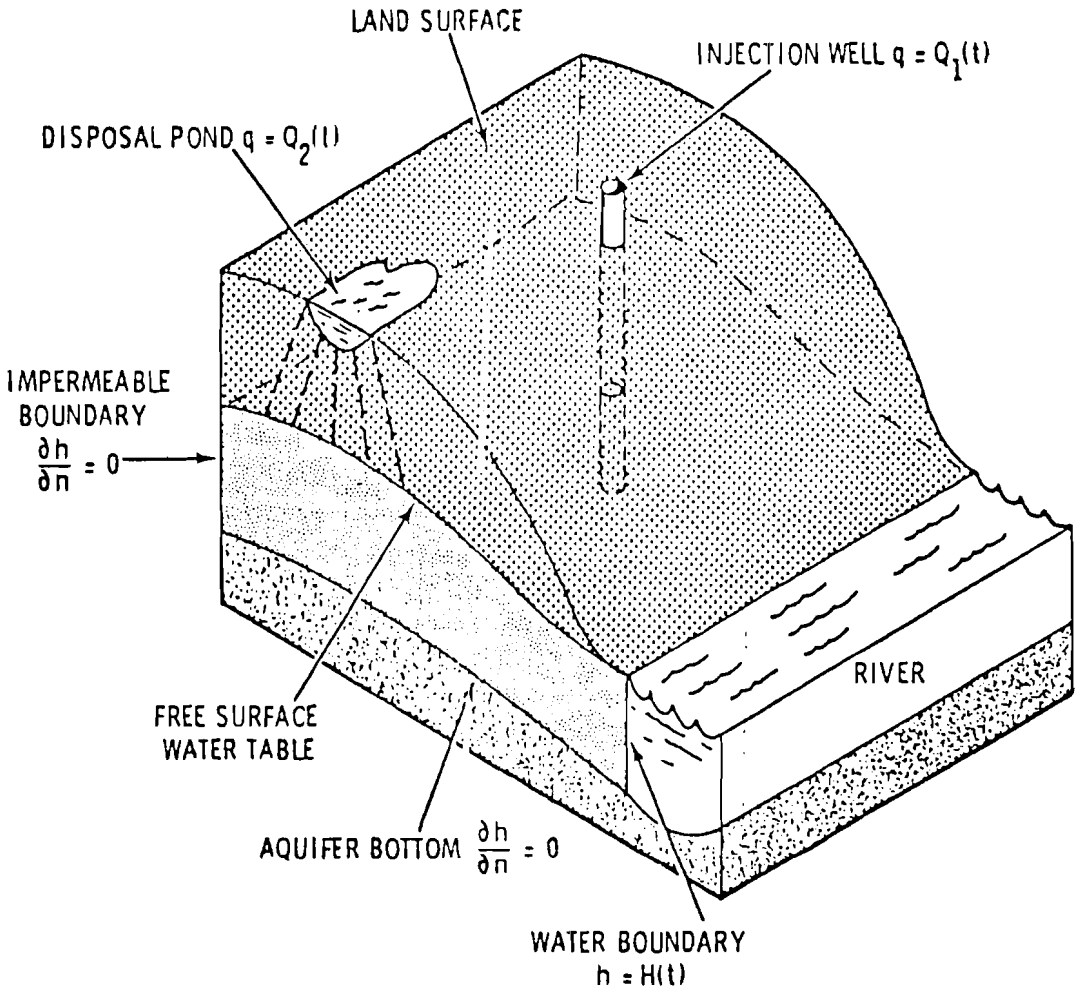

FIGURE 1. Illustration of an Unconfined Aquifer With Boundary Conditions

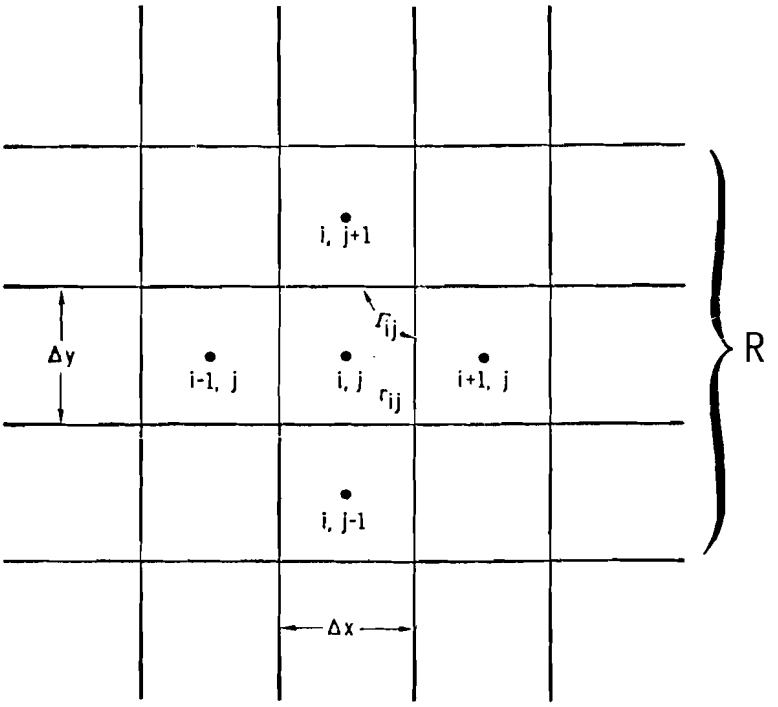

FIGURE 2. The Finite Difference Grid With the Nodal Numbering System

NUMERICAL FORMULATION OF THE SYSTEM EQUATIONS

A horizontal x-y coordinate grid system was adopted with uniform nodal spacing of 2000 feet. R represents the region of flow and r_{ij} the sub-area associated with node ij (see Figure 2).

Then the differential equation (Equation 11) is converted to finite difference form by integrating around the node area r_{ij}. Now

$$\iint_{r_{ij}} \left[\underline{\nabla} \cdot K(h - h^{o}) \underline{\nabla} h - \phi \frac{\partial h}{\partial t} + q' \, dxdy = 0 \right. \tag{14}$$

by Green's theorem in the first form,[6]

$$\iint_{r_{ij}} \underline{\nabla} \cdot K(h - h^{o}) \underline{\nabla} h dxdy = \oint_{\Gamma_{ij}} K(h - h^{o}) \frac{\partial h}{\partial n} ds \tag{15}$$

where n denotes the outward pointing normal to the curve Γ which bounds the area r_{ij}. The line integral is taken in the anti-clockwise direction. Using Equation 15, Equation 14 reduces to

$$\oint_{\Gamma_{ij}} K(h - h^{o})\frac{\partial h}{\partial n}ds - \iint_{r_{ij}} (\sigma\frac{\partial h}{\partial t} - q)dxdy = 0 \qquad (16)$$

In Figure 2 the corner points of the node area are at (i-1/2, j-1/2), (i+1/2, j-1/2), (i+1/2, j+1/2), and (i-1/2, j+1/2). The area of r_{ij} is $\Delta x\Delta y$. The integrals of Equation 16 are approximated as follows with the integral along Γ_{ij} divided into the integrals along the four sides of r_{ij}:

$$\int_{i-1/2,\ j-1/2}^{i+1/2,\ j-1/2} K(h - h^{o})\frac{\partial h}{\partial n}dx \simeq (K\Delta h)_{i,j-1/2}\ \frac{h_{ij} - h_{i,j-1}}{-\Delta y}\ \Delta x \qquad (17a)$$

$$\int_{i+1/2,\ j-1/2}^{i+1/2,\ j+1/2} K(h - h^{o})\frac{\partial h}{\partial n}dy \simeq (K\Delta h)_{i+1/2,\ j}\ \frac{h_{i+1,\ j} - h_{ij}}{\Delta x}\Delta y \qquad (17b)$$

$$\int_{i+1/2,\ j+1/2}^{i-1/2,\ j+1/2} K(h - h^{o})\frac{\partial h}{\partial n}dx \simeq (K\Delta h)_{i,\ j+1/2}\ \frac{h_{i,\ j+1} - h_{ij}}{\Delta y}\ \Delta x \qquad (17c)$$

$$\int_{i-1/2,\ j+1/2}^{i-1/2,\ j-1/2} K(h - h^{o})\frac{\partial h}{\partial n}dy \simeq (K\Delta h)_{i-1/2,\ j}\ \frac{h_{ij} - h_{i-1,\ j}}{-\Delta x}\ \Delta y \qquad (17d)$$

$$\iint_{r_{ij}} (+\sigma\frac{\partial h}{\partial t} - q)dxdy \simeq \sigma_{ij}\ \frac{h_{ij}^{n} - h_{ij}^{n-1}}{\Delta t}\ \Delta x\Delta y - q_{ij}\Delta x\Delta y \qquad (17e)$$

where

$$(K\Delta h)_{i,j-1/2} = 1/2(K_{ij}(h_{ij}^{n} - h_{ij}^{o}) + K_{i,j-1}\ (h_{i,j-1}^{n} - h_{ij}^{o})), \text{ etc.}$$

A fully implicit representation of the time derivative has been used in Equation 17e. Combining the above approximations results in the finite difference approximation to the Boussinesq equation for a square grid system, $\Delta x = \Delta y$:

$$-(K\Delta h)_{i-1/2,j}\, h^{n}_{i-1,j} + \left[(K\Delta h)_{i-1/2,j}+(K\Delta h)_{i+1/2,j}+(K\Delta h)_{i,j-1/2}\right.$$

$$\left.+(K\Delta h)_{i,j+1/2}+\sigma_{ij}\frac{(\Delta x)^2}{\Delta t}\right] h^{n}_{ij}-(K\Delta h)_{i+1/2,j}\, h^{n}_{i+1,j}$$

$$=(K\Delta h)_{i,j-1/2}\, h^{n}_{i,j-1}+(K\Delta h)_{i,j+1/2}\, h^{n}_{i,j+1}+\sigma_{ij}\frac{(\Delta x)^2}{\Delta t} h^{n-1}_{ij}+Q^{n-1}_{ij}(\Delta x)^2 \qquad (18)$$

1) For nodes on boundaries along which the hydraulic potential is specified, no calculation is needed; $h^{n}_{ij} = H^{n}_{ij}$, (19) which is given.

2) The impermeable boundaries of the region must be approximated in the grid system by shapes selected from Figure 3. This avoids right angles which cause stagnation points and singularities in the mathematical solution of the groundwater flow equation.

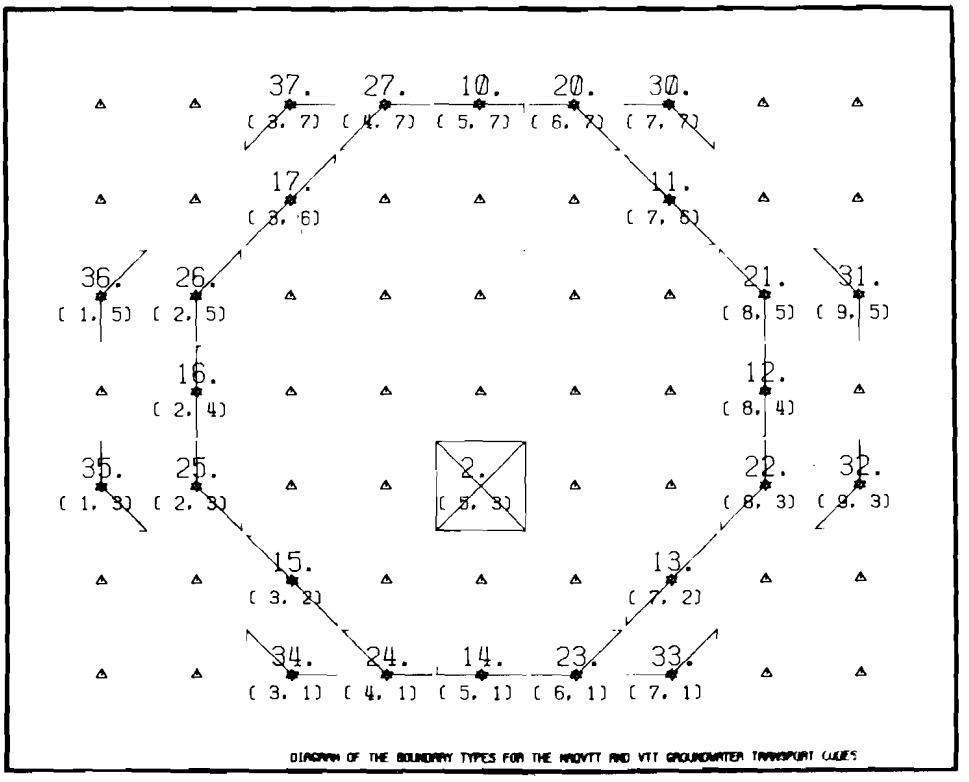

FIGURE 3. Schematic Showing Shapes and Rotation of Available Boundary Condition Types

The boundary conditions are put into finite difference form by applying the technique described above to a node area at the boundary of the region R. The boundary types are illustrated in Figure 3 and the associated nodal area r_{ij} can be either inside or outside the octagon. The finite difference equations are derived by setting the appropriate portions of the integral on Γ_{ij} in Equation 15 to zero when the segment is impermeable and by inputting $q'_{ij} = q_{ij}n$ when the flux across the segment is specified. In finite difference form, 24 different equations correspond to each of the different boundary point subregions illustrated in Figure 3. Either a specified flux or no flow can be imposed by each of the 24 equations.

3) The accretion term, whether infiltration or withdrawal, in finite difference form becomes $Q_{ij} = q_{ij}(\Delta x)^2$ (units L^3/T) to be specified at each node. Accretion at the fractional boundary nodes must have the nodal area properly reduced from $(\Delta x)^2$.

In summary, the partial differential equation and boundary conditions become a set of N finite difference equations, one for each node of the region R being modeled. The boundary conditions have been effectively absorbed into the equations for their respective boundary nodes.

It should be noted that the finite difference equations can be derived in the same form by other techniques, such as Taylor series expansions. The equations for nodes on impermeable boundaries are equivalent to those obtained by introduction of a point external to the region for purposes of forming the normal derivative.

CALCULATION PROCEDURE

The finite difference equations form an NxN matrix of equations in the form $\underline{\underline{A}}\underline{h} = \underline{b}$ for each row or column of nodes to be solved for the potentials, h^n_{ij}, at each time step, n, of the solution. For solutions of large systems of equations, some iterative technique is normally used to solve the system of equations.

A systematic treatment of iterative techniques according to Smith[7] is presented in Appendix A.

The finite difference representation of a linear parabolic partial differential equation on an nxm computational grid using a fully implicit method yields a matrix $\underline{\underline{A}}$ of the form

$$\underline{\underline{A}} = \begin{bmatrix} \underline{\underline{A}}_{11} & \underline{\underline{A}}_{12} & & & 0 \\ \underline{\underline{A}}_{21} & \underline{\underline{A}}_{22} & \underline{\underline{A}}_{23} & & \\ & \underline{\underline{A}}_{32} & \underline{\underline{A}}_{33} & \underline{\underline{A}}_{34} & \\ & & \ddots & \ddots & \ddots \\ 0 & & & \ddots & \ddots \end{bmatrix}$$

where elements a_{ij} or $\underline{\underline{A}}_{ij}$ are zero if $|i-j| \neq 0$ or 1.

This matrix may be partitioned so that the diagonal matrices $\underline{\underline{A}}_{ij}$ are tri-diagonal nxn submatrices and the off diagonal matrices are diagonal matrices. The partitioned matrix equation is tri-diagonal in the submatrices with each submatrix relating to a given line of nodal points in the finite difference mesh. This means that only three lines have to be accessible at any given time in the computations, which enables many nodes to be used to cover a simulation area before exceeding computer storage capacity. The method of successive over-relaxation, called successive line over-relaxation, or SLOR technique, can be applied to the partitioned matrix equation.

The Boussinesq equation is nonlinear, which makes the elements of the matrix $\underline{\underline{A}}$ functions of the values of h_{ij}

$$\underline{\underline{A}}(\underline{h})\underline{h} = \underline{b}.$$

The nonlinear SLOR technique is represented by the following equation:

$$\underline{h}^{k+1} = [\underline{\underline{D}}(\underline{h}^k) - \omega\underline{\underline{L}}(\underline{h}^k)]^{-1}\left[\left(\underline{\underline{D}}(\underline{h}^k)\ (1-\omega) + \omega\underline{\underline{U}}(\underline{h}^k)\right)\underline{h}^k + \left[\left(\underline{\underline{D}}(\underline{h}^k) - \omega\underline{\underline{L}}(\underline{h}^k)\right)\right]^{-1}\ \omega\underline{b}\right] \qquad (20)$$

where $\underline{\underline{D}}$, $\underline{\underline{U}}$, $\underline{\underline{L}}$, $\underline{h}$, $\underline{b}$ are the partitioned matrices and vectors. The equation is "linearized" by evaluating the components of $\underline{\underline{D}}$, $\underline{\underline{U}}$, and $\underline{\underline{L}}$ with the new values of h_{ij} as soon as they are available after a row computation.

The nonlinearity prevents the determination of an analytical optimum over-relaxation factor. An empirical factor may be

calculated by fitting a parabola to three computed values of iterations required versus relaxation factor, then locating the minimum. This requires equally spaced time steps, however.

A fully implicit formulation was used for the finite difference equations derived from the Boussinesq equation and boundary conditions. This determines the coefficients of the elements in $\underline{\underline{A}}$ and $\underline{b}$.

COLLECTION AND PREPARATION OF THE INPUT DATA

As mentioned in the second section of this report, the following items are necessary to specify a particular groundwater flow system to be simulated:

1) adoption of a grid system, subsequent location of lateral boundaries, and their types;

2) the time variation of the potential along the water boundaries;

3) the locations and flow rates of infiltration and their variations with time;

4) the surface that represents the aquifer bottom;

5) the initial potential distribution, time = 0, for the simulation (see Boundary and Initial Conditions); and

6) hydraulic conductivity and storage coefficient distributions.

This section will cover the first five items. BNWL-1706, The Transmissivity Iterative Calculation Routine - Theory and Numerical Implementation, covers item six.

The basic grid system selected was a Cartesian x,y coordinate system with the y axis oriented north-south and a 2,000 foot spacing between the nodes in either direction. The origin was at 69,000 feet south and 109,000 feet west in the Hanford Reservation coordinate grid. The boundary points were chosen to be those closest to the Columbia and Yakima River bank contours from the U. S. Geological Survey topographical maps, and the estimated outcrop contour boundaries for the basalts that form the Rattlesnake Hills, Yakima Ridge, Umtanum Ridge, Gable Mountain, and Gable Butte. These outcrop boundaries occur where the bedrock rises above the water table. Figure 4 shows the boundaries of the Hanford

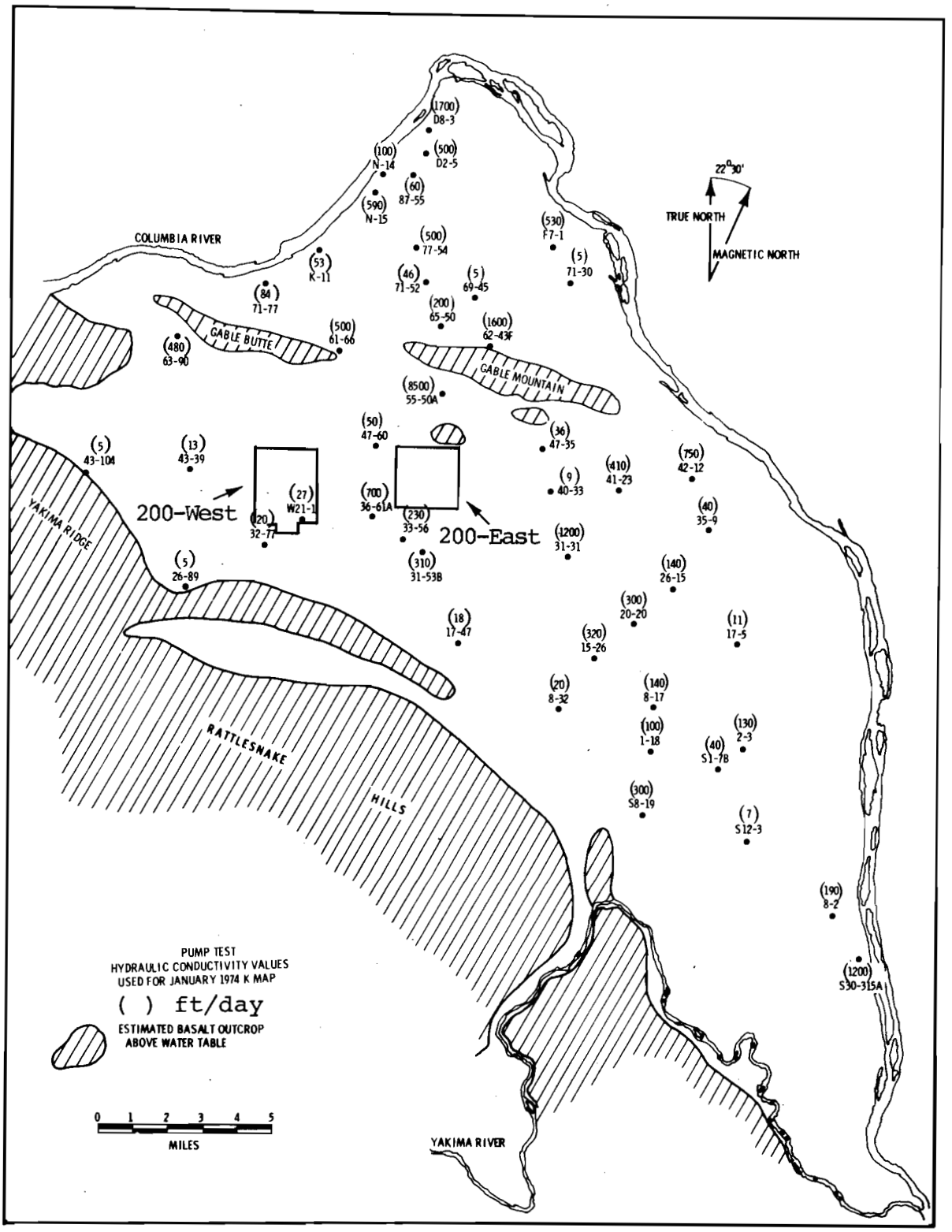

FIGURE 4. Locations and Values of Measured Hydraulic Conductivities for the Hanford Unconfined Aquifer

Reservation. The portion of the free surface aquifer which extends into the region between Yakima Ridge and Rattlesnake Mountain was not included in the model.

Along the impermeable boundaries, the appropriate boundary condition types were selected from those shown in Figure 3. Along the Cold Creek Valley recharge boundary between Umtanum Ridge and Yakima Ridge, the inflow was approximated and held constant. Gable Mountain, Gable Butte and Yakima Ridge were assumed impermeable to flow.

The time variation of the Columbia River elevation profile was predicted by a routine which used a fit curve of historical river stage versus flow rate values. Appendix C discusses the routine used to calculate elevations during years where data exist. This program is described in BNWL-1704,[8] Variable Thickness Transient Program User's Manual. Intermediate nodes were linearly interpolated. River flow rate data were obtained on a monthly basis for the period simulated. Thus, average elevations along the Columbia River for each month were employed. The Yakima River was held constant at an average elevation profile.

The infiltration flows resulted from disposal of process water to various facilities near the 200 separations plants (200 East Area and 200 West Area, Figure 4). Each disposed site facility was assigned to a node or a group of nodes based on its location and extent. There was also infiltration from the cooling water systems at the reactor areas near N-14. The quantities of flow from the 200 Areas were taken to be the reported discharge volumes on a monthly basis over the period of simulation. No attempt was made to take into account the time lag involved for flow from the ground surface to the water table. This seems justified since the large volume discharges do not vary widely.

The aquifer bottom surface was established by information from driller's logs, geological cross sections from those logs, and clay content analyses of certain soil samples. The aquifer bottom was assumed to be impermeable for the purposes of this simulation. Very little is known about locations and quantities of possible flow through the unconfined aquifer bottom. In some areas the bottom was taken as the bedrock or basalt while in others a thick layer of low permeability clay forms the bottom. The information from the discrete well locations was contoured and then digitized to provide the aquifer bottom elevation at each computational node of the system. The digitizer program is described in BNWL-1652,[9] Use of a Graphic Digitizer Program to Interpolate Matrix Grid Values.

Many of the wells on the Hanford Reservation do not reach the bottom of the unconfined aquifer, so much intuitive interpolation had to be done in preparing the aquifer bottom contour surface shown in Figure 5. Any new data collected will help improve the definition of this surface.

An initial potential surface or groundwater table elevation surface for the test simulation was contoured from water level measurements at the wells shown in Figure 4. This March 1968 surface was also digitized for input to the VTT model program (Figure 6).

The aquifer properties were determined by a fairly complex calculation procedure which is described in BNWL-1706.[10] The Transmissivity Iterative Calculation Routine - Theory and Numerical Implementation. The hydraulic conductivity distribution (Figure 7) was digitized and input to the model. At this time the capability to calculate a storage coefficient distribution did not exist, so a constant value of 0.1 was assumed.

With the above information in the proper format on the input data files, the Variable Thickness Transient Model was ready to simulate the groundwater flow for the Hanford Reservation for the period March 1968 through September 1973. The starting and ending times were dictated by availability of measured potential data for comparison and evaluation of the model's performance. The September 1973 potential map is shown in Figure 8. BNWL-1704, The VTT Program User's Manual describes the formats for all essential input data mentioned above.

TESTING AND VERIFICATION OF THE VTT MODEL

A test simulation of the groundwater flow under the Hanford Reservation was made for the period March 1968 through September 1973. The results were excellent where good field data exist and generally poorer in less well-known areas. Boundary and infiltration conditions were changed monthly to correspond with historical conditions. The following time sequence was used each month: first, second, third, fifth, and twentieth days. The shorter steps were used at the beginning of the month because conditions were changed on the first day of each month. This approach tended to equalize the number of iterations necessary for each time step calculation. The simulation was evaluated by comparison of the calculated with the potential surface interpreted for September 1973. The difference was calculated node-by-node and the results grouped by class. Table 1 shows the tabulated results for this comparison. Hydrograph comparisons at specific wells were also made.

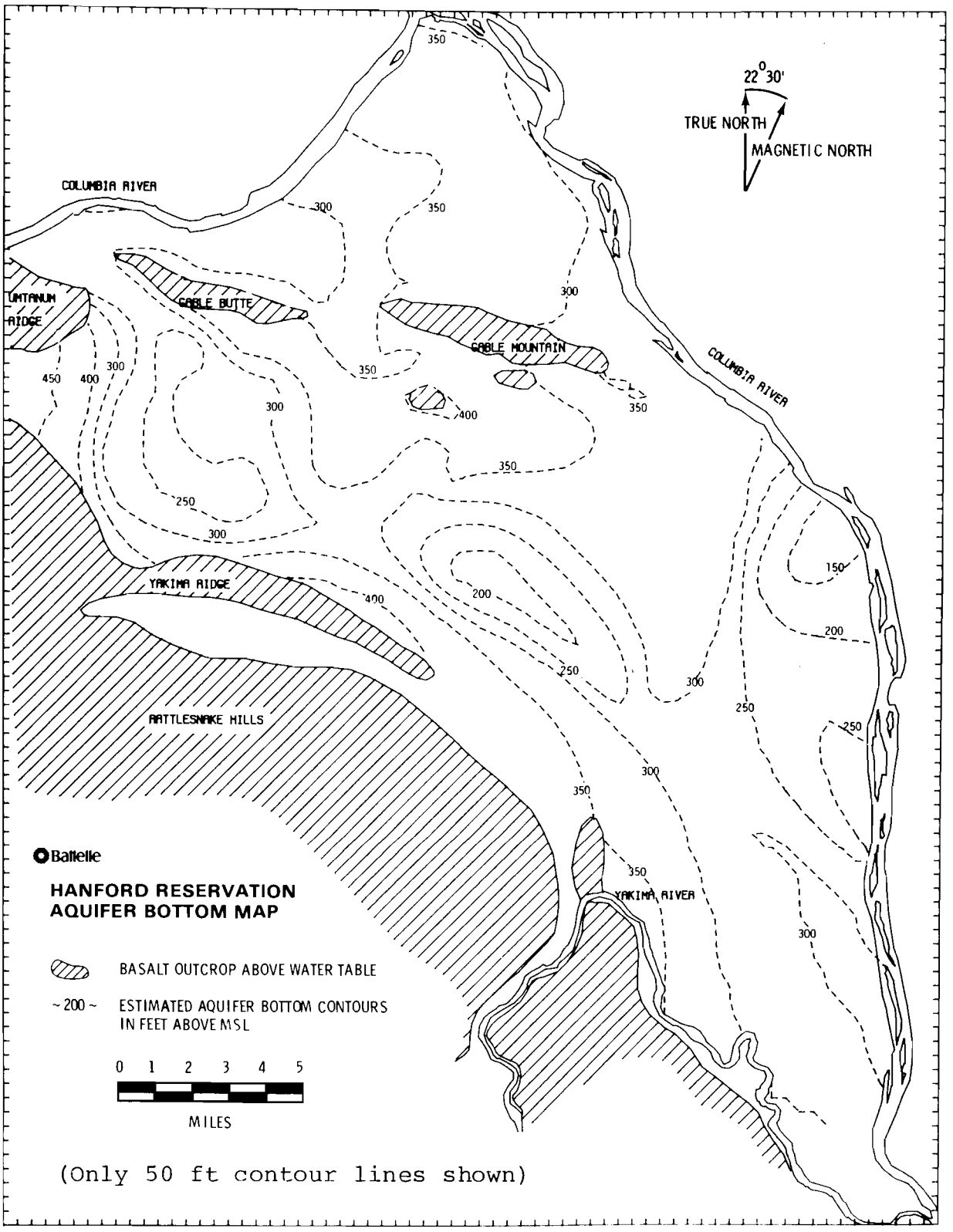

FIGURE 5. Elevation of the Hanford Unconfined Aquifer Bottom Used in Calculating the Hydraulic Conductivity Distribution

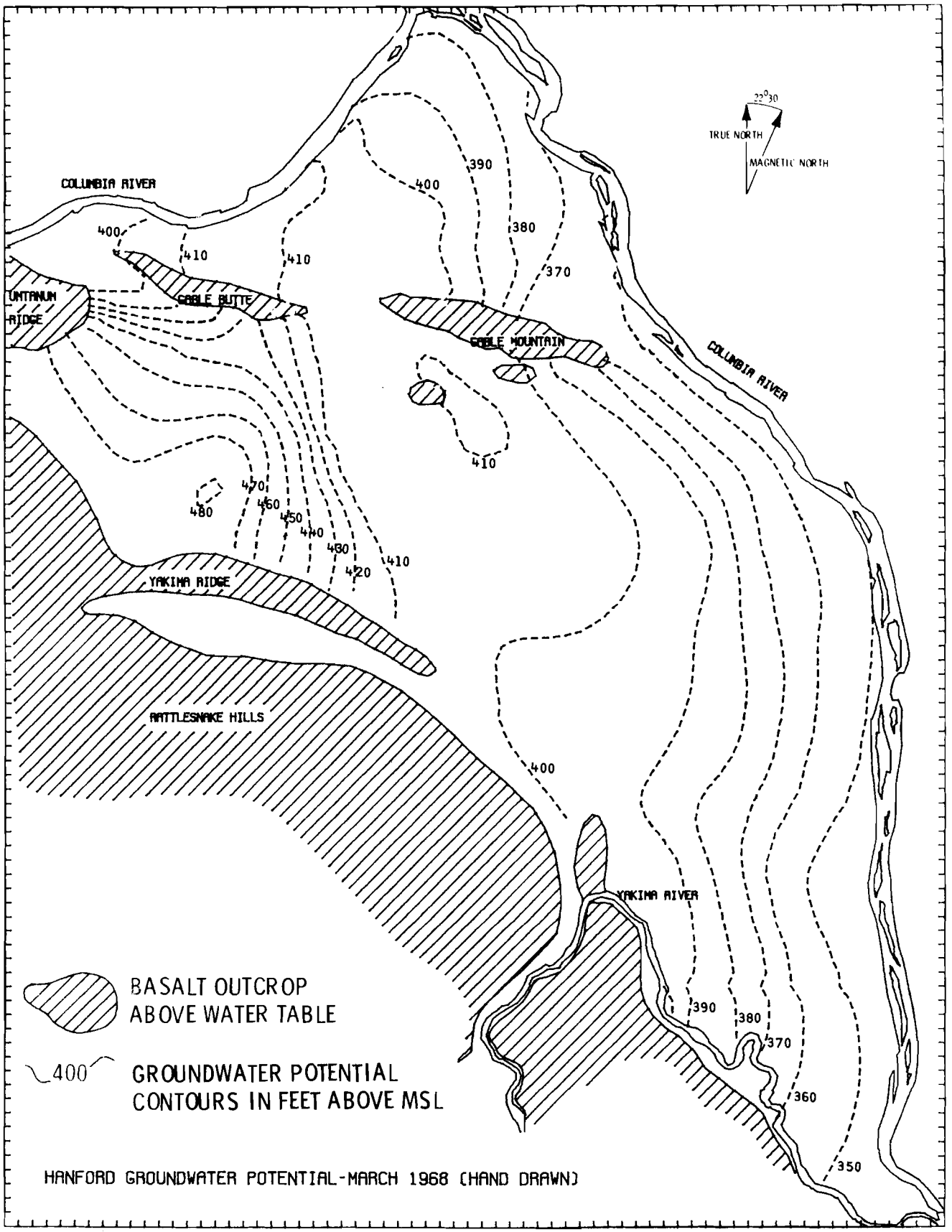

FIGURE 6. Initial Potential Surface for Transient Simulation

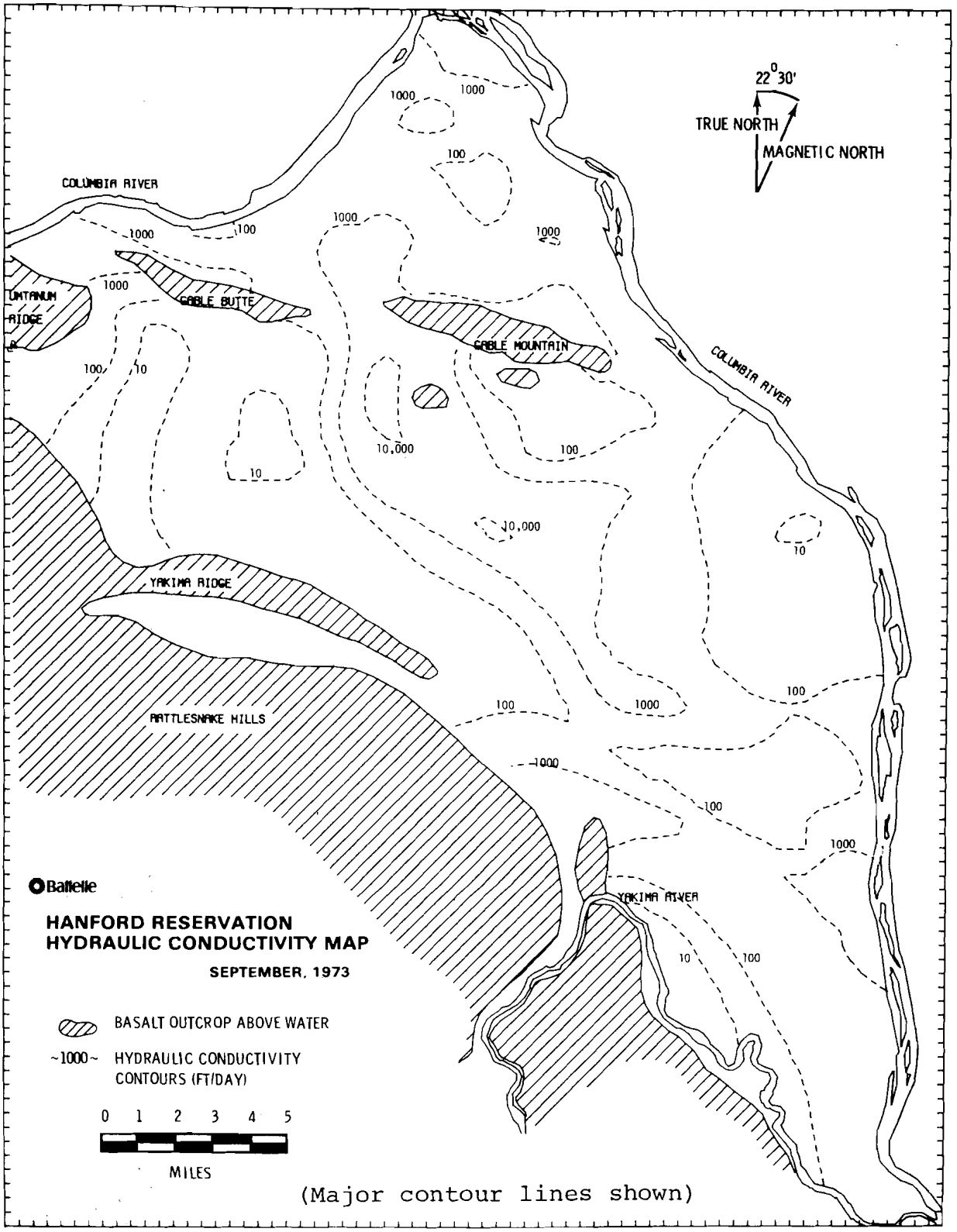

FIGURE 7. Hydraulic Conductivity Calculated Assuming a Transient Groundwater System

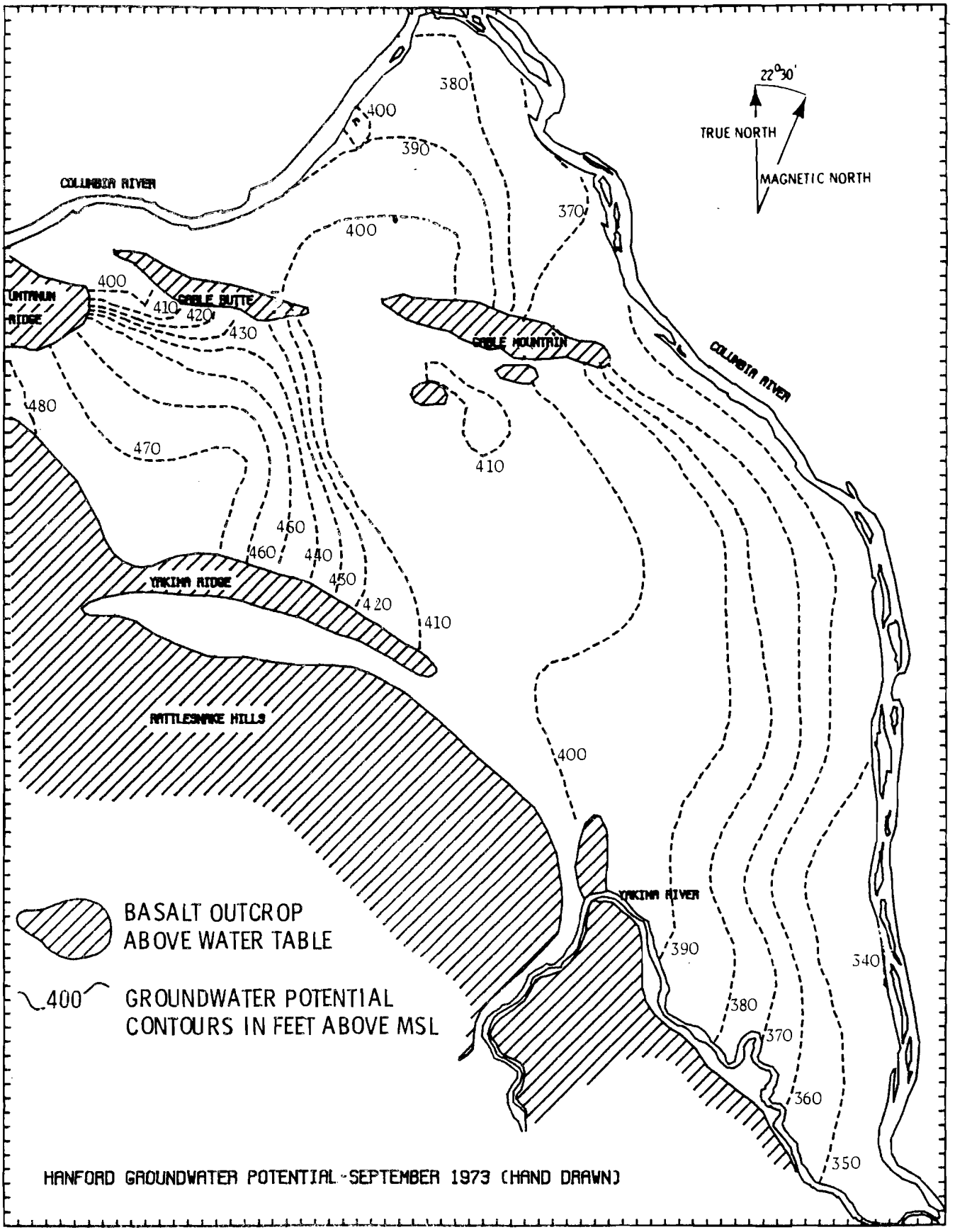

FIGURE 8. Groundwater Potentials Interpreted from ∿250 Field Measurements Used in Calculating the Hydraulic Conductivity Distribution

TABLE 1. Differences Between Calculated and Observed Groundwater Potentials at the End of the 5-Year Simulation Period at Model Nodes

Class	Range in Feet	Absolute Difference	% of Nodes	Positive Difference	% of Nodes	Negative Difference	% of Nodes
A	0.000 - 1.000	572	23.744	298	12.370	274	11.374
B	1.000 - 2.000	413	17.144	139	5.770	274	11.374
C	2.000 - 4.000	594	24.658	89	3.694	505	20.963
D	4.000 - 8.000	463	19.220	78	3.238	385	15.982
E	8.000 -15.000	240	9.963	20	0.830	220	9.132
F	15.000 -35.000	127	5.272	3	0.125	124	5.147
		2409		627	26.027	1782	73.973

Max. difference - 34.2 ft
Average difference - 4.2 ft
RMS difference - 6.3 ft

Figure 9 is a map of the distribution of the difference classes for September 1973. The letter class designation in Table 1 is printed on Figure 9 to show the distribution of the simulation quality. Figure 9 also shows the sign of the deviation between calculated and interpreted potentials. A positive sign means the predicted elevation was above the interpreted elevation in September 1973. From the maps and the statistics, the following evaluations of the simulation's quality can be made:

1) The agreement was excellent in the area southeast of the 200 East Area, where the aquifer parameters were known best.

2) The two areas of greatest discrepancy are to the east of Umtanum Ridge and to the east of Rattlesnake Mountain. Areas 3 and 1 respectively in Figure 9. Hydraulic conductivities were extrapolated into these areas and the recharge flows from the two boundaries are only estimates. At the east end of Gable Mountain (Area 5) a small area of poor fitting also occurs. This one appears due to a bad estimate of the aquifer bottom. It is clear that both the recharge flows, bottom elevations and the conductivities need to be field measured in these areas. The other large area of poor model performance is in the high gradient area on the east side of the 200 West Area mound (Area 4). The hydraulic conductivity appears to be too high in this area. Other minor areas of poor agreement occur near Gable Butte and Gable Mountain, where hand extrapolation of the hydraulic conductivity distribution was necessary because the TIR could not be used in these areas.

3) In general, model-predicted potentials were too low in the northern part of the Reservation.

Figures 10A and B show the calculated and hand-contoured potential surface using field data for September 1973 in isometric views. Figure 11 shows the calculated September 1973 water table map.

Certain contouring errors of interpretation can be present in the digitized versions of the measured potential surfaces. This will affect the quality of the comparison with the VTT predicted values. Comparison of the model simulation with the historical hydrographs at selected well sites eliminates this problem at the expense of areal visualization of the simulation quality. Looking at the time history of the measured versus simulated water table elevations can give further insight into the VTT model's behavior. The two types of comparisons, in space and in time, are complementary.

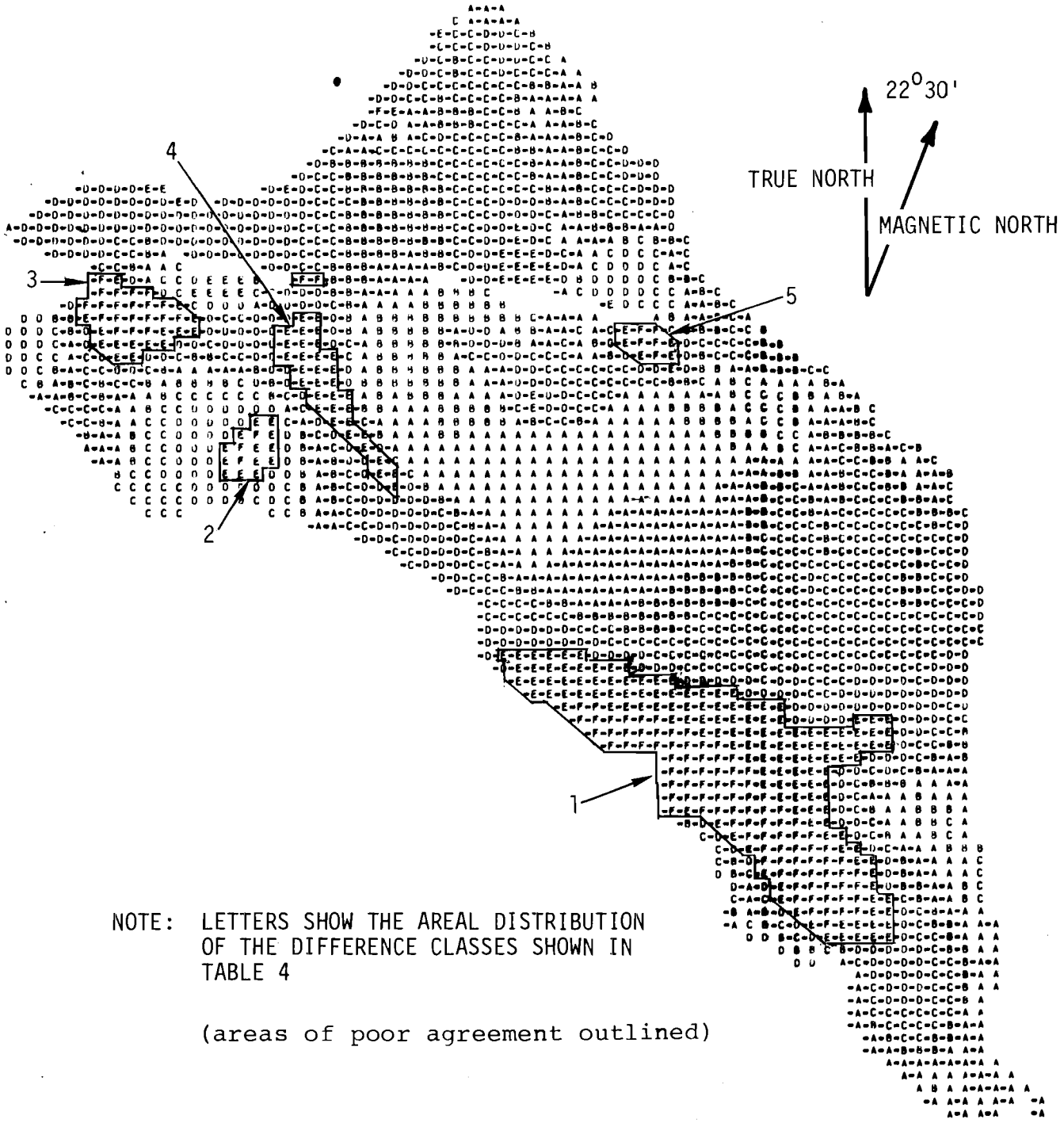

NOTE: LETTERS SHOW THE AREAL DISTRIBUTION OF THE DIFFERENCE CLASSES SHOWN IN TABLE 4

(areas of poor agreement outlined)

FIGURE 9. Difference Classes Comparing the September 1973 Calculated Water Table With the Water Table for the Same Month Interpreted From Field Measurements

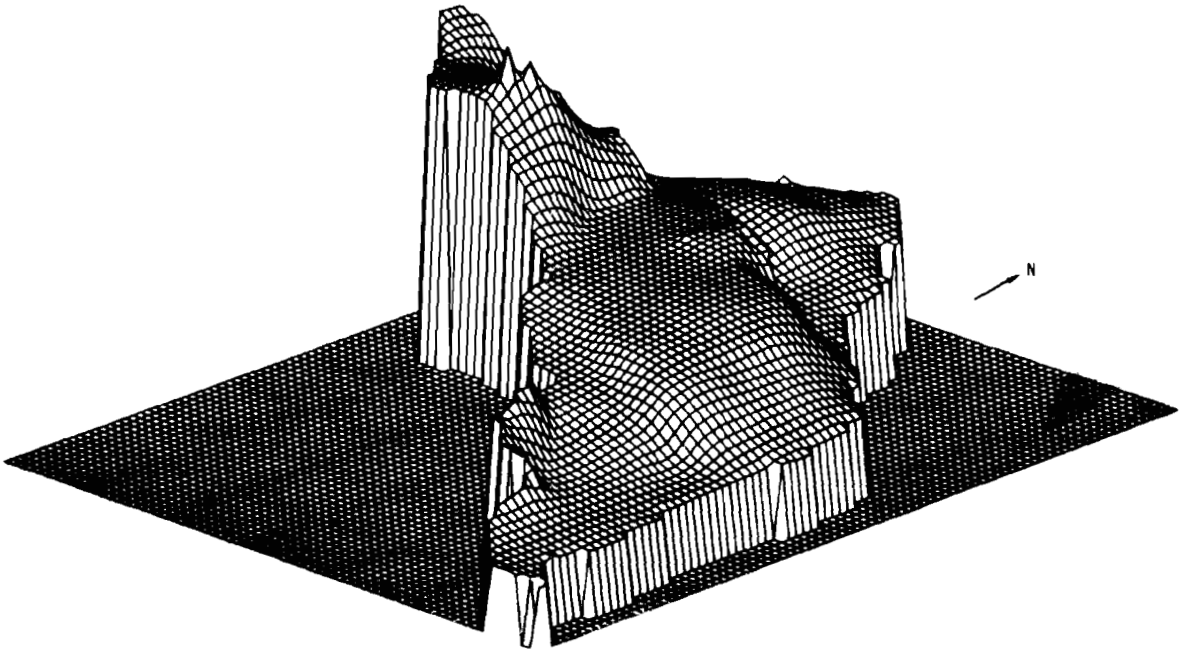

FIGURE 10A. Isometric Plot of the Calculated Groundwater Potentials for the Hanford Unconfined Aquifer, September 1973

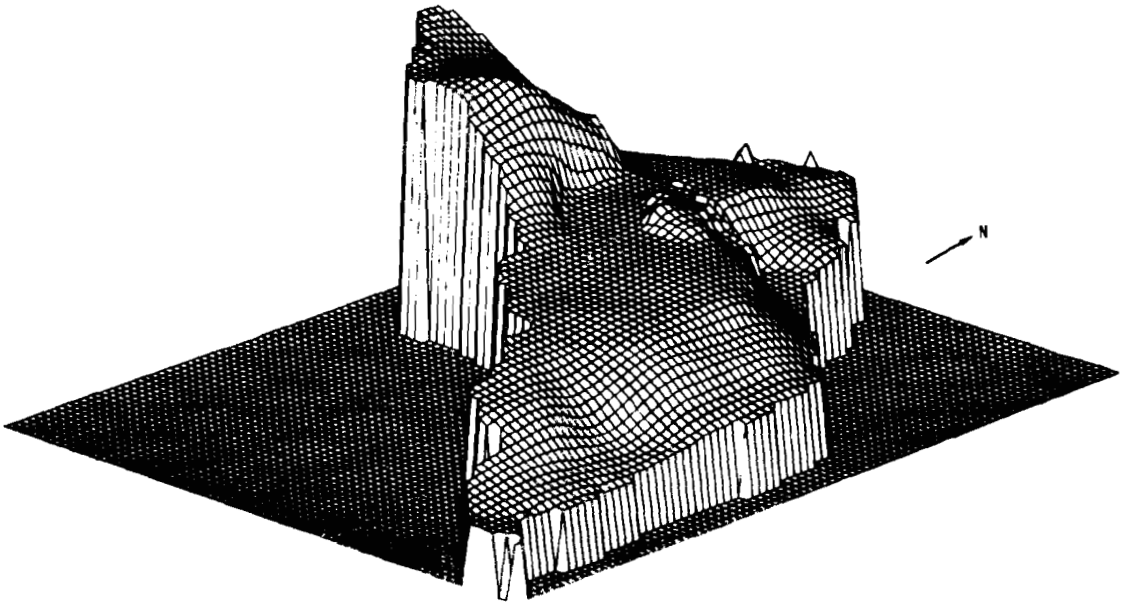

FIGURE 10B. Isometric Plot of the Hand-Contoured Groundwater Potentials Data for the Hanford Unconfined Aquifer, September 1973

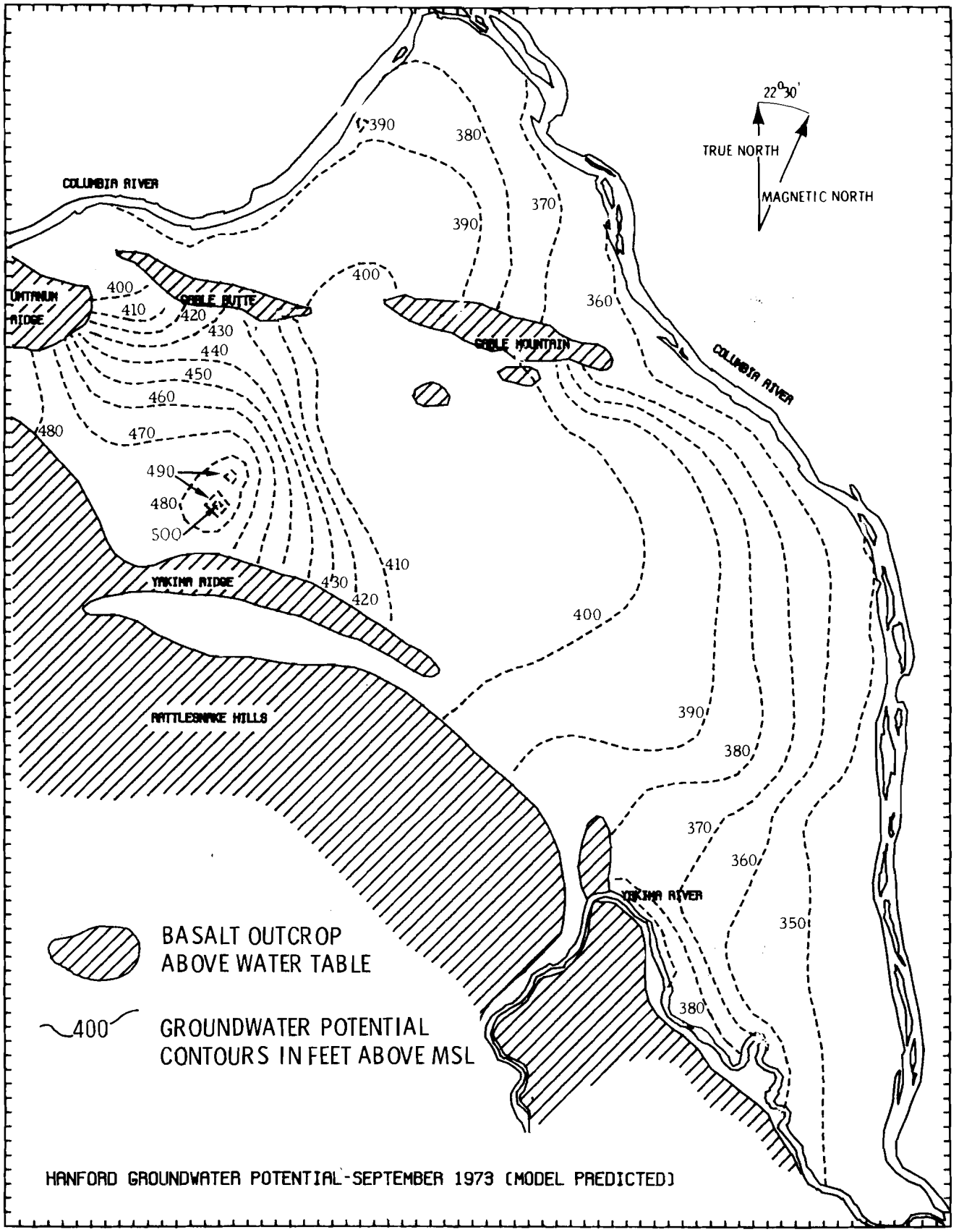

FIGURE 11. Calculated Water Table From VTT Simulation for September 1973

Figure 12 shows a sample hydrograph display of a measured and calculated water elevation at a representative well on the Hanford Reservation. The line segments from 1968-1973 are VTT model results. The interpretations of the quality of the simulation given above are amply illustrated by these hydrographs.

The sensitivity of the VTT model to the various parameters in a heterogeneous system is difficult to determine directly because the potential, h_{ij}, at each node is a function of the parameters and potentials at all of the neighboring nodes. However, several synthetic test cases were run to obtain a qualitative feeling for the model's sensitivity to the various parameters. These cases are described in detail in Appendix B. The conclusions reached were as follows:

For these limited cases, one would conclude that a change of 10 times the value in K results in a 2 fold change in potential. A 100 percent change in storage coefficient results in only a 10 percent change in potential. Increasing the aquifer bottom elevation resulted in a one-fourth to one-third of that increase in the potential surface. Thus, resulting potentials were more sensitive to variations in hydraulic conductivity and aquifer bottom elevation than to storage coefficient in these synthetic cases. Because of the diffusive nature of the groundwater flow system, any change in the input parameters produces a somewhat attenuated change in the resultant potentials (water table elevations). The magnitude of any induced change is highly dependent on the current values of all of the other parameters. No single group of numbers can quantify the VTT model's sensitivity over the heterogeneous Hanford Reservation. A more complete sensitivity study has been undertaken which should delineate the relationship of the different parameters.

CONCLUSIONS

The Variable Thickness Transient Model of groundwater flow in the unconfined aquifer underlying the Hanford Reservation has been developed, tested and verified. The capability of the model to simulate horizontal flow with time varying boundary conditions, complex boundary shapes and a heterogeneous distribution of aquifer properties has been demonstrated.

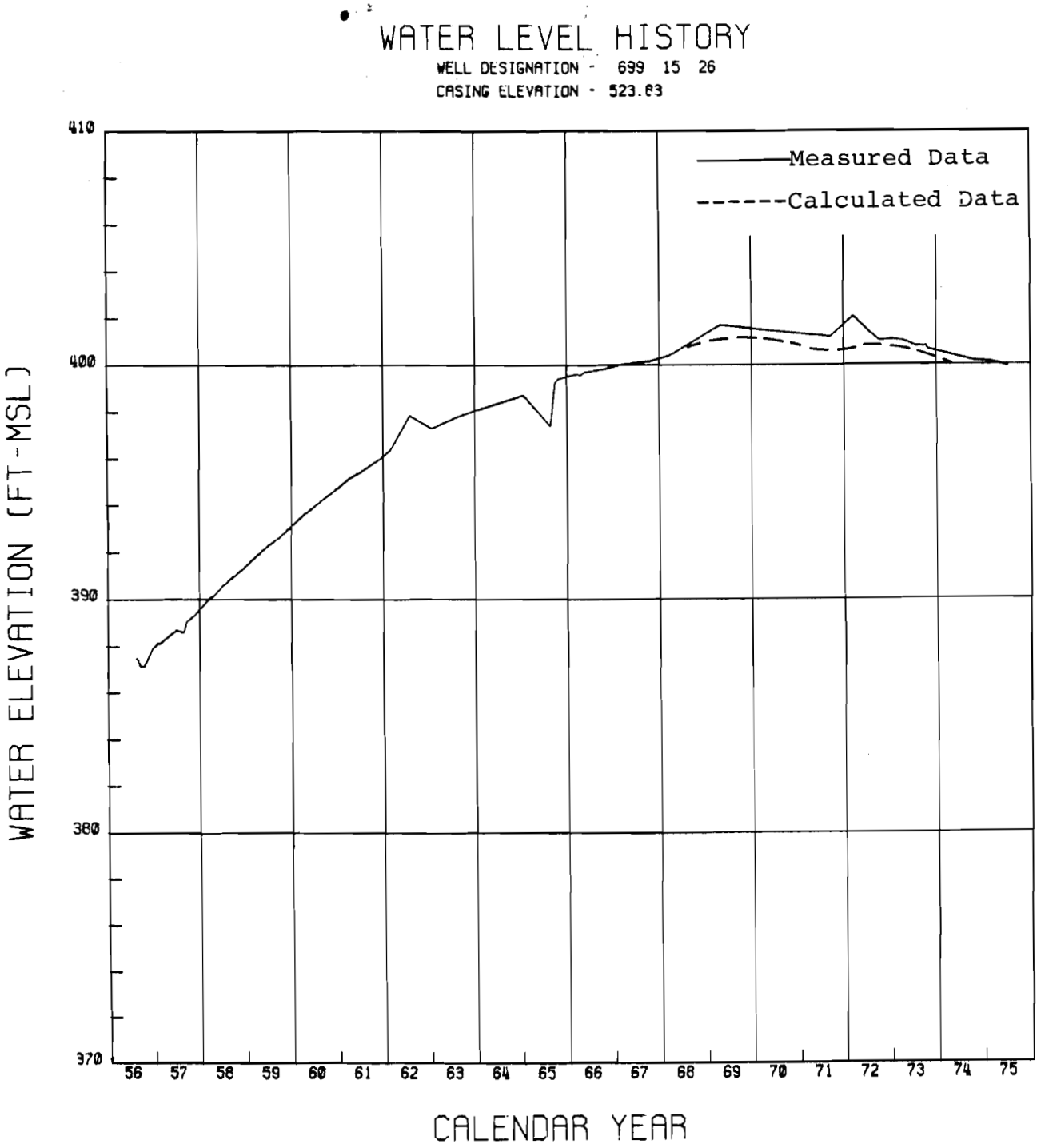

FIGURE 12. Measured and Calculated Well Hydrograph

ACKNOWLEDGMENTS

This research was sponsored by the Ground-Water Management Section, Research Department, Atlantic Richfield Hanford Company. The authors are grateful for the editorial comments and suggestions of R. W. Nelson, Boeing Computer Services, Inc. and direction and review assistance of R. A. Arnett, Senior Hydrologist, and Dr. R. A. Deju, Manager, Ground water Management Section.

REFERENCES

1. Stoker, J. J., Water Waves, Interscience, New York, 1957.

2. Bear, J., D. Zaslavsky, and D. Irmay, "Physical Principles of Water PErcolation and Seepage." UNESCO, Arid Zone Research, 29, 1968.

3. Polubarinova-Kochina, P. Ya., Theory of Ground Water Movement. (Trans. by R. J. M. DeWiest), Princeton University Press, Princeton, New Jersey, 1962.

4. DeWiest, R. J. M., ec., Flow Through Porous Media. Academic Press, New York, 1969.

5. Boussinesq, J. J., "Recherches Tĥeoriques sur l'écoulement des Nappes d'Eau Infiltrées dans le Sol et sur Débit des Sources." Jour. de Mathematiques Pures et Appliquees, Series 5, 10, 5-78, 1903, pp 363-394, 1904.

6. Kellogg, O. D., "Foundations of Potential Theory." Dover, New York, 1954.

7. Smith, G. D., Numerical Solution of Partial Differential Equations. Oxford University Press, London, 1965.

8. DeMier, W. V., A. E. Reisenauer and K. L. Kipp, "Variable Thick Transient Groundwater Flow Model - User's Manual", BNWL-1704, Battelle-Northwest, Richland, WA, 1974.

9. Friedrichs, D. R. "A graphic Digitizer Program to Interpolate Matrix Grid Values, User's Manual, BNWL-1652, Battelle-Northwest, Richland, WA, 1972.

10. Cearlock, D. B., K. L. Kipp, and D. R. Friedrichs, "The Transmissivity Iterative Calculation Routine - Theory and Numerical Implementation", BNWL-1706, Battelle-Northwest, Richland, WA, 1975.

APPENDIX A

A SYSTEMATIC TREATMENT OF ITERATIVE TECHNIQUES

APPENDIX A

The following systematic treatment of iterative techniques is according to Smith.[7] For linear systems, $\underline{\underline{A}}\underline{x} = \underline{b}$. (1) The basic technique is to write $\underline{\underline{A}}$ as the difference of two matrices $\underline{\underline{B}}$ and $\underline{\underline{C}}$ where $\underline{\underline{B}}$ is easily invertible.

$$\underline{\underline{A}}\underline{x} = \underline{\underline{B}}\underline{x} - \underline{\underline{C}}\underline{x} = \underline{b} \tag{2}$$

or

$$\underline{x} = \underline{\underline{B}}^{-1}\,\underline{\underline{C}}\underline{x} + \underline{\underline{B}}^{-1}\,\underline{b}. \tag{3}$$

The iterative technique is to guess $\underline{x}^{o}$ for the solution and define $\underline{x}^{k+1} = \underline{\underline{B}}^{-1}\,\underline{\underline{C}}\underline{x}^{k} + \underline{\underline{B}}^{-1}\,\underline{b}$. $k = 0, 1, 2, \ldots$ The process will converge whenever the eigenvalue of largest modulus of $\underline{\underline{B}}^{-1}\,\underline{\underline{C}}$ has modulus less than 1.

Elliptic and parabolic differential equations give finite difference systems that can be written as $\underline{\underline{A}} = \underline{\underline{D}} - \underline{\underline{U}} - \underline{\underline{L}}$ where $\underline{\underline{D}}$ is a diagonal matrix, $\underline{\underline{U}}$ has non-zero entries only on certain super-diagonals, and $\underline{\underline{L}}$ has non-zero entries only on certain sub-diagonals. Equation 1 becomes $(\underline{\underline{D}} - \underline{\underline{L}} - \underline{\underline{U}})\underline{x} = \underline{b}$ so $\underline{x}$ satisfies $\underline{x} = \underline{\underline{D}}^{-1}(\underline{\underline{L}} + \underline{\underline{U}})\underline{x} + \underline{\underline{D}}^{-1}\,\underline{b}$. The Jacobi method is defined by $\underline{x}^{k+1} = \underline{\underline{D}}^{-1}(\underline{\underline{L}} + \underline{\underline{U}})\underline{x}^{k} + \underline{\underline{D}}^{-1}\,\underline{b}$. This technique requires storage of both $\underline{x}^{k}$ and $\underline{x}^{k+1}$. By using all the improved values as soon as they are computed, less storage is required and faster convergence is obtained. The Gauss-Seidel method can be defined by:

$$\underline{x}^{k+1} = \underline{\underline{D}}^{-1}\,\underline{\underline{L}}\,\underline{x}^{k+1} + \underline{\underline{D}}^{-1}\,\underline{\underline{U}}\,\underline{x}^{k} + \underline{\underline{D}}^{-1}\,\underline{b}.$$

This can be written as

$$(\underline{\underline{I}} - \underline{\underline{D}}^{-1}\,\underline{\underline{L}})\underline{x}^{k+1} = \underline{\underline{D}}^{-1}\,\underline{\underline{D}}\,\underline{x}^{k} + \underline{\underline{D}}^{-1}\,\underline{b}$$

giving

$$\underline{x}^{k+1} = (\underline{\underline{I}} - \underline{\underline{D}}^{-1}\,\underline{\underline{L}})^{-1}\,\underline{\underline{D}}^{-1}\,\underline{\underline{U}}\,\underline{x}^{k} + (\underline{\underline{I}} - \underline{\underline{D}}^{-1}\,\underline{\underline{L}})^{-1}\,\underline{\underline{D}}^{-1}\,\underline{b}.$$

When $\underline{x}$ is not the exact solution of $\underline{\underline{A}}\underline{x} = \underline{b}$, the difference is called the residual vector $\underline{r}$. A relaxation method calculates the components of $\underline{r}$ for an initial guess, $\underline{x}^{o}$, for $\underline{x}$, then reduces the residuals to zero in an iterative fashion by making appropriate changes in the components of $\underline{x}$. These changes are called relaxations. One systematic order for proceeding through the relaxations is

$$\underline{r}^{k} = \underline{b} - \underline{\underline{D}}\underline{x}^{k} + \underline{\underline{U}}\underline{x}^{k} + \underline{\underline{L}}\underline{x}^{k+1} \tag{4}$$

where $\underline{r}^k$ is the residual from the vector $\underline{x}^k$. If $\underline{x}^{k+1}$ is picked so that the vector $\underline{r}^k$ is reduced to zero, the equation becomes that of the Gauss-Seidel procedure. The displacement vector $\underline{d}$ is defined as the change in the vector $\underline{x}$ over one iteration $\underline{d} = \underline{x}^{k+1} - \underline{x}^k$, or

$$\underline{x}^{k+1} = \underline{x}^k + \underline{d}. \tag{5}$$

The displacement vector $\underline{d}$ for the Gauss-Seidel scheme satisfies the following equation:

$$(\underline{\underline{I}} - \underline{\underline{D}}^{-1}\,\underline{\underline{L}})\underline{d} = \underline{\underline{D}}^{-1}\,\underline{\underline{U}}\underline{x}^k + \underline{\underline{D}}^{-1}\,\underline{b}. \tag{6}$$

Subtraction of Equation 6 from 4 and using 5 yields

$$\underline{\underline{D}}^{-1}\,\underline{r}^k - (\underline{\underline{I}} - \underline{\underline{D}}^{-1}\,\underline{\underline{L}})\underline{d} = \underline{\underline{D}}^{-1}\,\underline{\underline{L}}\,\underline{d}.$$

Therefore, $\underline{\underline{D}}^{-1}\,\underline{r}^k = \underline{d}$; i.e., the displacement vector at each step in the Gauss-Seidel method is identically equal to the residual vector times the inverse of the diagonal elements of the $\underline{\underline{A}}$ matrix.

Again the rate of convergence can be improved by making the displacement vector some multiple of the residual vector; i.e., $x^{k+1} = x^k + \omega D^{-1} r^k$ where $\omega \geq 0$, a real number. This is called under-relaxation for $\omega < 1$ and over-relaxation for $\omega > 1$. The defining equation for the successive over-relaxation technique is thus $\underline{\underline{D}}\underline{x}^{k+1} = \underline{\underline{D}}\underline{x}^k + \omega(\underline{\underline{L}}\underline{x}^{k+1} + \underline{\underline{U}}\underline{x}^k + \underline{b} - \underline{\underline{D}}\underline{x}^k)$. Rearranging gives:

$$\underline{x}^{k+1} = (\underline{\underline{D}} - \omega\underline{\underline{L}})^{-1}[\underline{\underline{D}}(1 - \omega) + \omega\underline{\underline{U}}]\underline{x}^k + (\underline{\underline{D}} - \omega\underline{\underline{L}})^{-1}\,\omega\underline{b}. \tag{7}$$

It has been proved that the method converges for $0 < \omega < 2$ whenever $\underline{\underline{A}}$ is symmetric and positive definite. Optimum relaxation factors, ω_{opt}, can be derived theoretically for linear systems.

All three of the above schemes are stationary iterative processes because the coefficients of $\underline{x}$ in the recursion formulas are independent of the iteration step value, k. This is not true for nonlinear systems of equations.

APPENDIX B

VTT ERROR AND SENSITIVITY ANALYSIS ON SYNTHETIC SURFACES*

*Note that a more complete sensitivity study is underway.

APPENDIX B

For the VTT model, a qualitative sensitivity analysis was done with synthetic surfaces, all of which had the following common parameters unless noted:

Area = 8900X8900 ft^2 Grid spacing = 100 ft

Boundary flow rate = $1x10^6$ ft^3/day

Injection flow rate = 1×10^6 ft^3/day

Hydraulic conductivity (K) = 1000 ft/day Storage coefficient (σ) = 0.2

The aquifer parameters were chosen because they are in the range used on the Hanford model and still allow reasonable variation.

The effects of variations in the several parameters were illustrated by the following sets of surfaces. The time plane at t=3 days is illustrated for each set.

Set 1: Storage coefficient variation: Figure B-1 shows the surface at t=3 days for σ = 0.2. This surface was previously used for testing the accuracy of the transmissivity routine. Figure B-2 shows the same time plane for σ = 0.08. The elevation of the peak of the mound is 34.8 ft in Figure B-1 and 36.9 ft in Figure B-2. The contours start at 10 ft and are at 5 ft intervals. The sharper peak for the lower storage coefficient case is apparent. However, the percent change in peak elevation between the two cases is about 5.5% while the change in storage coefficient is 60%.

Set 2: Variation in hydraulic conductivity: Figure B-1 shows the surface for K=1000 ft/day. Figure B-3 shows the surface for K=100 ft/day. The elevation of the mound has increased by almost a factor of two to 64 ft in Figure B-3 while the hydraulic conductivity has changed by an order of magnitude. As for the storage coefficient, the calculated potentials are not proportionally sensitive to changes in hydraulic conductivity.

A second case was run with the hydraulic conductivity increased to 1500 ft/day over a portion of the area (see sketch below).

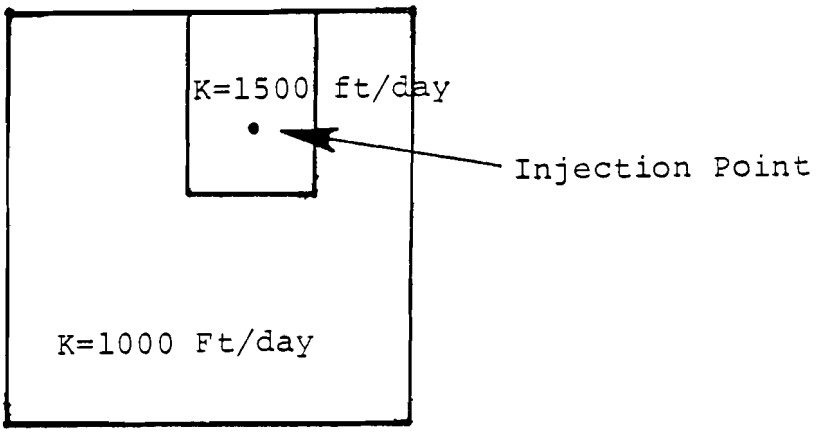

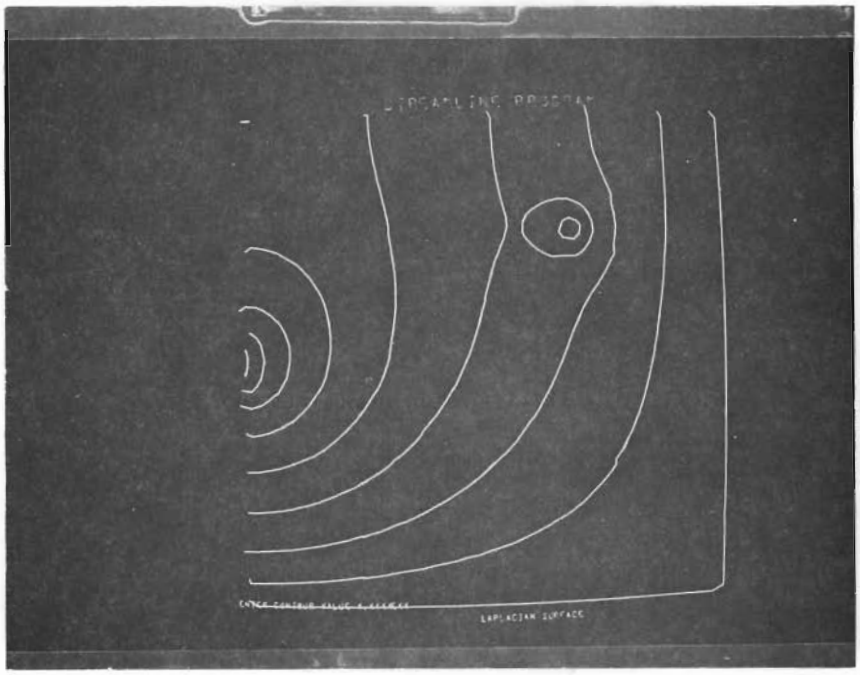

FIGURE B-1. Effects of Parameter Variation on Synthetic Surface, t = 3 Days, σ = 0.2

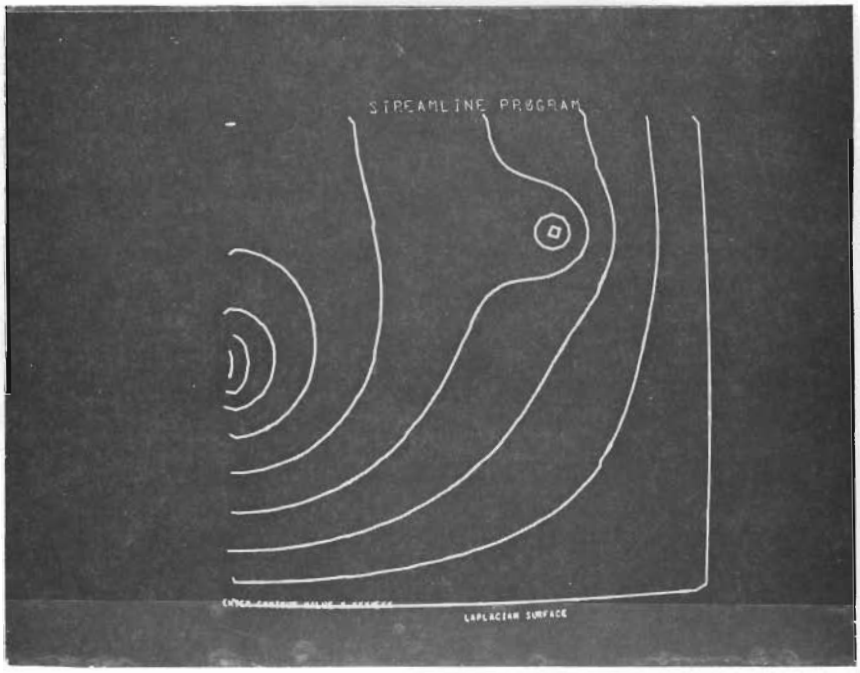

FIGURE B-2. Effects of Parameter Variation on Synthetic Surface, t = 3 Days, σ = 0.08

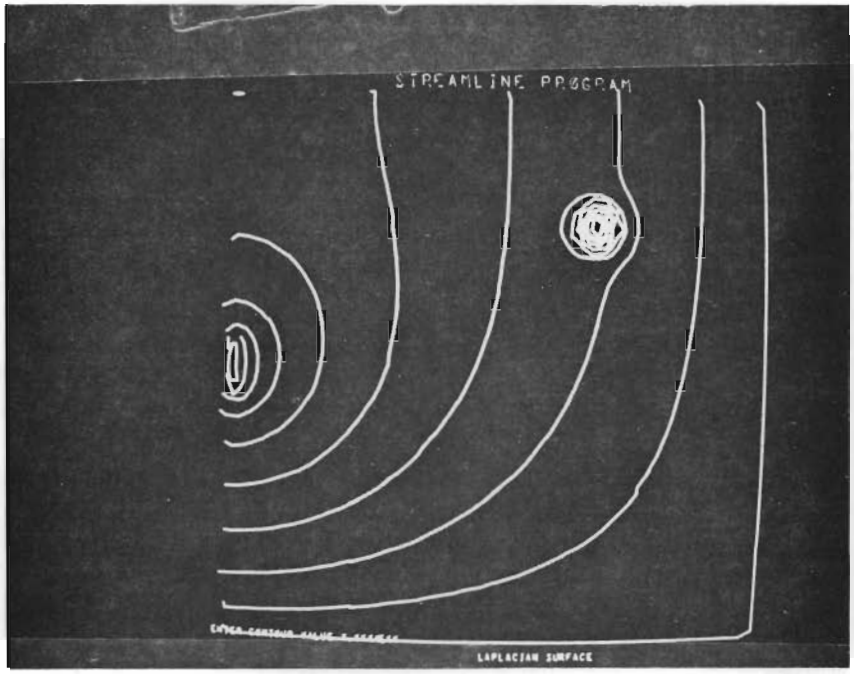

FIGURE B-3. Effects of Parameter Variation on Synthetic Surface, K = 100 Ft/Day, t = 3 Days

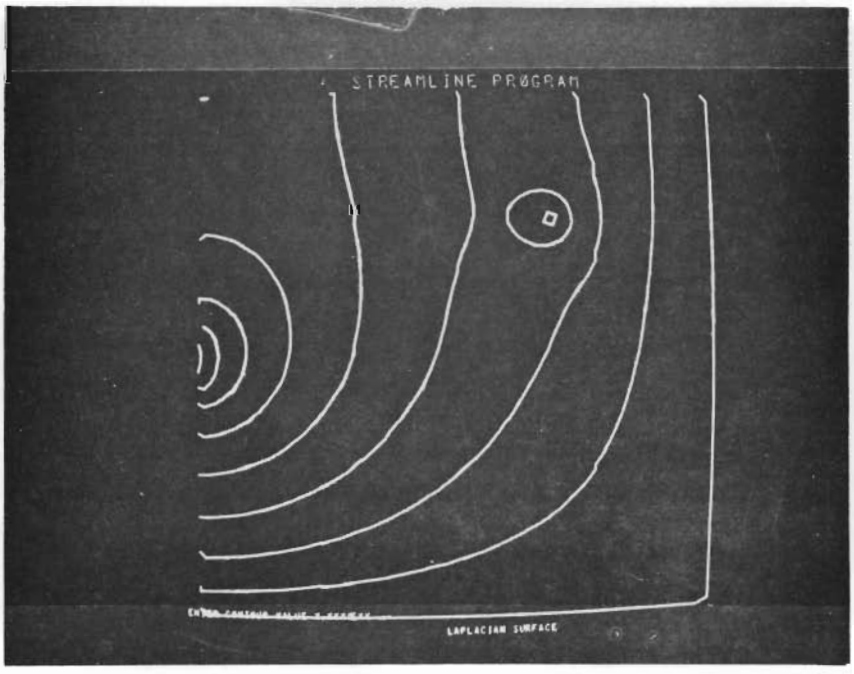

FIGURE B-4. Effects of Parameter VAriation on Synthetic Surface, Block Hydraulic Conductivity Distribution Where K = 1000 and 1500 Ft/Day, t = 3 Days

Figure B-4 shows the three day time plane results. The peak of the mound was reduced about 10% from the K-1000 ft/day case (i.e., from 34.8 ft to 31.6 ft).

Set 3: Variation in the aquifer bottom elevation: For all previous cases the aquifer bottom was set at zero elevation. One set of surfaces was run with the following bottom elevation profile.

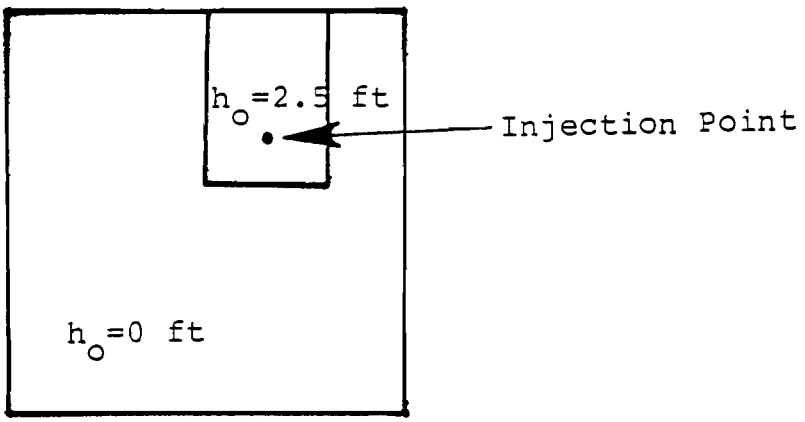

Figure B-5 shows the peak of the mound increased to 35.5 ft, about 1/4 of the change in the aquifer bottom elevation beneath the mound. A second case was run with the following aquifer bottom profile.

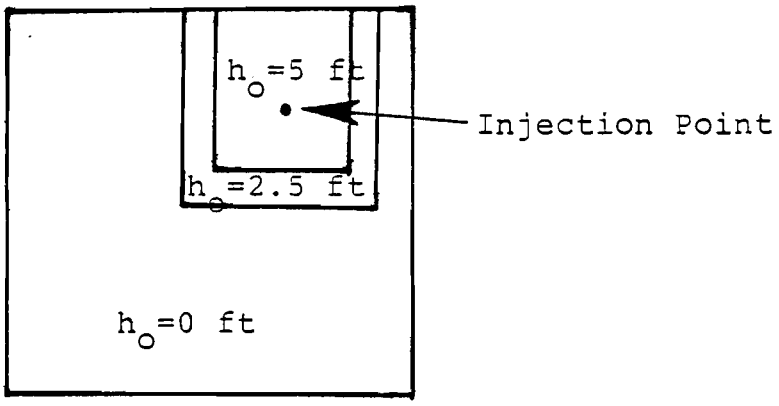

Figure B-6 shows the peak elevation of the mound increased to 36.6 ft, about 1/3 of the aquifer bottom elevation increase beneath the mound.

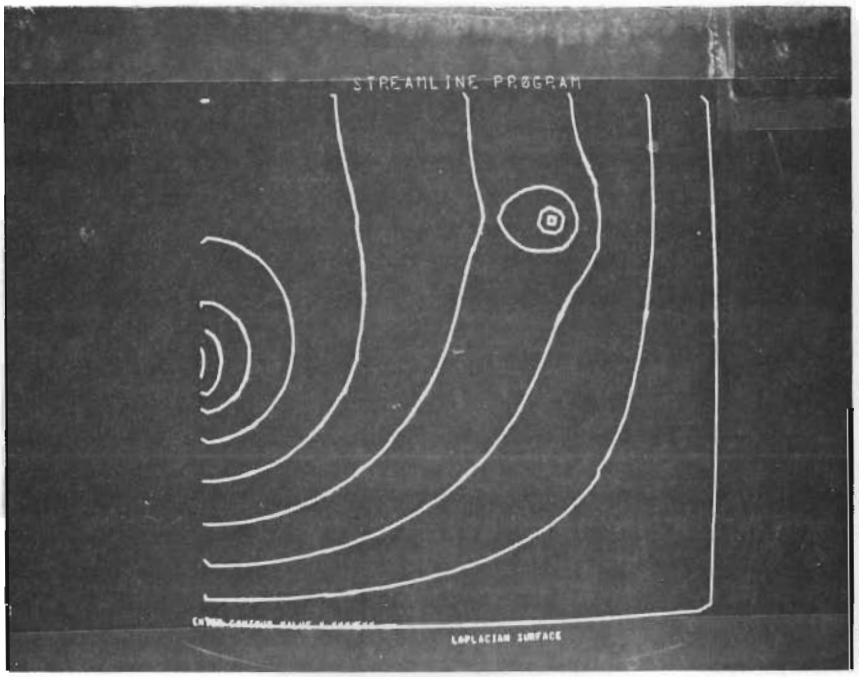

FIGURE B-5. Effects of Parameter Variation on Synthetic Surface, h_o = 2.5 and 0 Ft, t = 3 Days

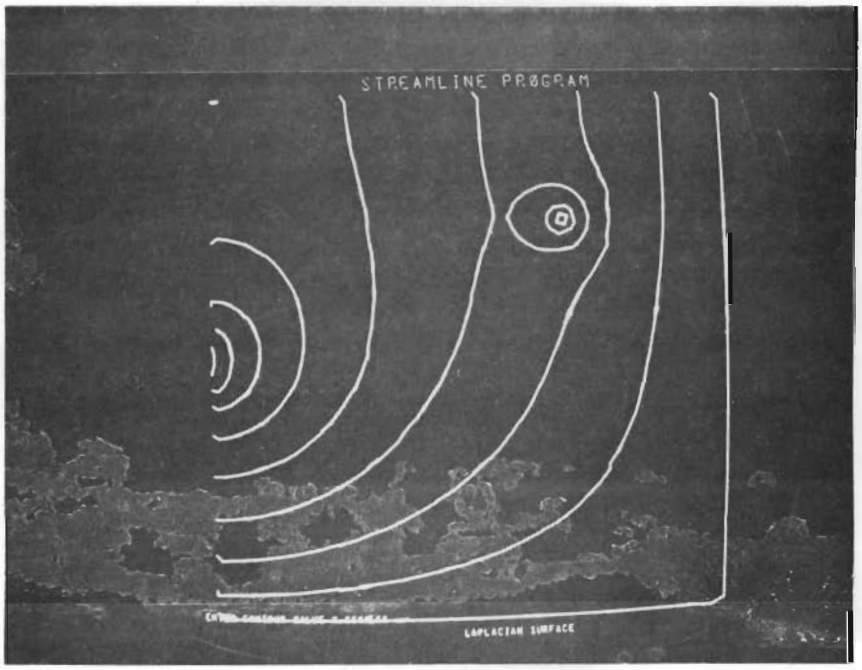

FIGURE B-6. Effects of Parameter Variation on Synthetic Surface, h_o = 5, 2.5 and 0 Ft, t = 3 Days

As might be expected, because of the diffusive nature of the groundwater flow system any change in the input parameters produces a somewhat attenuated change in the resultant potentials or water table elevations. The magnitude of any induced change is highly dependent upon the values of all of the other parameters. Consequently, the sensitivity of the calculated potentials for the Hanford Reservation to parameter variations will vary with position and time.

APPENDIX C

RIVER ELEVATION CALCULATIONS

APPENDIX C

The VTT model requires that the potential (a function of river mile and flow rate) be specified at each boundary node along the river. A total of 18,360 values are needed to specify these potentials at monthly intervals for the period 1968-1973. There are 255 nodes at the river boundary in the 1000 ft grid system. Every other node is used in the 2000 ft grid. To eliminate the problems associated with generating, checking, indexing, storing and reading such a data file, a subroutine has been written which computes boundary potentials.

The subroutine computes river elevations as a function of flow rate over the range 6×10^9 to 3×10^{10} ft^3/day. The functions were developed from field measurements of river elevation and flow rate and are second-to-fifth order polynomials, depending on the region of the river covered. They give elevations at every fifth river mile beginning at mile 335. Potentials at nodes not on five mile marks are found by interpolation. Table C-1 shows how the interpolation factors are derived from a sample reach of river. The x,y coordinates represent nodes in the 2000 ft grid. Taking the side of the square to be one unit, the point-to-point distances are summed from node 38,79 to node 31,87 (12.9 units). The interpolation factor for node x,y is the point-to-point distance from node 38,79 to node x,y divided by the total distance, 12.9. A special table enables the computer to determine which polynomial is to be applied to a given boundary node.

TABLE C-1. Example of PK Construction

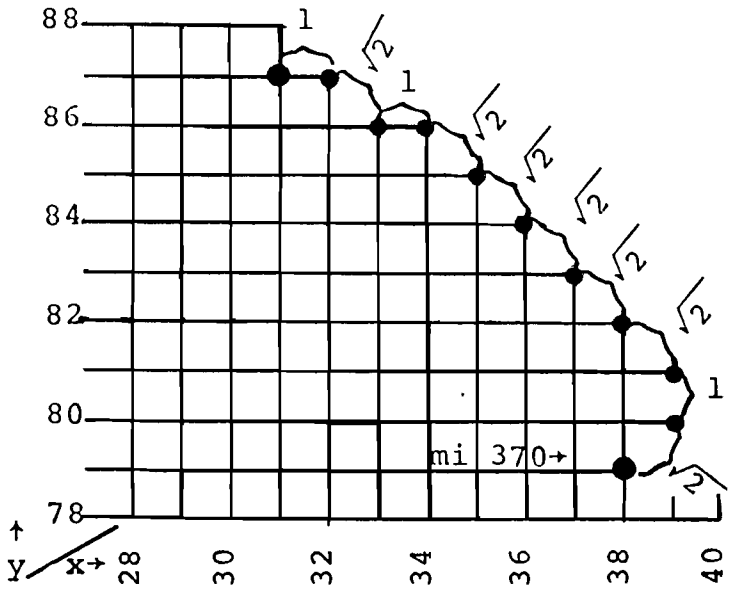

Total distance point to point from river mile 370 to river mile 375 = (3 + 7 $\sqrt{2}$) units = 12.9

NODE	INTERPOLATION FACTOR
38,79	0.0
39,80	$\sqrt{2}/12.9 = 0.1096$
39,81	$(1 + \sqrt{2})/12.9$
38,82	$(1 + 2\sqrt{2})/12.9$
37,83	$(1 + 3\sqrt{2})/12.9$
36,84	$(1 + 4\sqrt{2})/12.9$
35,85	$(1 + 5\sqrt{2})/12.9$
34,86	$(1 + 6\sqrt{2})/12.9$
33,86	$(2 + 6\sqrt{2})/12.9$
32,87	$(2 + 7\sqrt{2})/12.9$
31,87	$(3 + 7\sqrt{2})/12.9$

APPENDIX D

DEVELOPMENT OF THE BOUSSINESQ EQUATION

APPENDIX D

Let x,y,z be the coordinates of a fluid particle, then dx/dt, dy/dt and dz/dt are components of pore velocity and the Darcian seepage velocities in these terms are:

$$q_x = \sigma \frac{dx}{dt} \tag{1}$$

$$q_y = \sigma \frac{dy}{dt} \tag{2}$$

$$q_z = \sigma \frac{dz}{dt} \tag{3}$$

Now if we let $z = h(x,y,t)$ represent the coordinate of the free surface and formally differentiate with respect to time we have:

$$\frac{\partial z}{\partial t} = \frac{\partial h}{\partial x}\frac{dx}{dt} + \frac{\partial h}{\partial y}\frac{dy}{dt} + \frac{\partial h}{\partial t} \tag{4}$$

Substituting the above expressions for Darcian velocities and rearranging, we have:

$$\sigma \frac{\partial h}{\partial t} + q_x \frac{\partial h}{\partial x} + q_y \frac{\partial h}{\partial y} - q_z(h) = 0 \tag{5}$$

The Dupuit assumptions may be simply stated as:

- $\phi(x,y,z,t) \underset{\sim}{\approx} \phi(x,y,\bar{z},t)$ where $\bar{z}$ = average height of the water particles above the reference datum (i.e. variations of ϕ with z are negligible).
- Horizontal velocities do not vary with z (this implies that the slope of the water table is slight).

Continuing, we assume that we are completely saturated and that the water density, ρ, is a constant, we have Equation 2 of the main text for our continuity equation or:

$$\frac{\partial q_x}{\partial x} + \frac{\partial q_y}{\partial y} + \frac{\partial q_z}{\partial z} = 0 \tag{6}$$

Now since we wish to average in the z direction, we must integrate this equation from the base of the aquifer to the free surface or:

$$q_z\Big|_{z=h^o}^{z=h} = q_z(h) = -(h-h^o)\left(\frac{\partial q_x}{\partial x} + \frac{\partial q_y}{\partial y}\right) \tag{7}$$

Since $\phi = p/\gamma + z$ and we know that at the free surface that $p = 0$, then $\phi = z$. Using this result along with the first Dupuit assumption and our earlier equation ($z = h(x,y,t)$), we have:

$$h(x,y,t) = \phi(x,y,\bar{z},t) \tag{8}$$

From this result Darcy's law can be rewritten as:

$$q_x = -K \frac{\partial h}{\partial x} \tag{9}$$

$$q_y = -K \frac{\partial h}{\partial y} \tag{10}$$

where:

$K(x,y)$ = vertically averaged value of hydraulic conductivity at location (x,y).

Substituting Equations 9 and 10 into Equation 5, we have:

$$\sigma\frac{\partial h}{\partial t} - K\left[\left(\frac{\partial h}{\partial x}\right)^2 + \left(\frac{\partial h}{\partial y}\right)^2\right] - q_z(h) = 0 \tag{11}$$

Now replacing $q_z(h)$ with the expression given in Equation 7, we have:

$$\sigma\frac{\partial h}{\partial t} - K\left[\left(\frac{\partial h}{\partial x}\right)^2 + \left(\frac{\partial h}{\partial y}\right)^2\right] - (h-h^o)\left[\frac{\partial}{\partial x}\left(K\frac{\partial h}{\partial x}\right) + \frac{\partial}{\partial y}\left(K\frac{\partial h}{\partial y}\right)\right] = 0 \tag{12}$$

Rearranging Equation 12, we have:

$$\sigma\frac{\partial h}{\partial t} - \frac{\partial}{\partial x}\left(K(h-h_b)\frac{\partial h}{\partial x}\right) - \frac{\partial}{\partial y}\left(K(h-h^o)\frac{\partial h}{\partial y}\right) = 0 \tag{13}$$

To this point for simplicity the accretion term has been neglected. Adding in the accretion term q' and rewriting Equation 13 in terms of the two-dimensional $\underline{\nabla}$ (x,y) gradient operation, we have the Boussinesq equation for unsteady flow in an unconfined aquifer (Equation 11 of the main text):

$$\underline{\nabla} \cdot K(h-h^o)\ \underline{\nabla}h = \sigma\frac{\partial h}{\partial t} - q' \tag{14}$$

DISTRIBUTION

No. of Copies	Off-Site
1	Chicago Patent Group A. A. Churm
215	Energy Research and Development Administration Technical Information Center
2	Energy Research and Development Administration Headquarters Waste Management and Transportation Division Germantown, Maryland 20767 Owen P. Gormley Chief, Waste Facilities Branch Robert W. Ramsey, Jr. Chief, Development Branch
2	Nuclear Regulatory Commission Directorate of Regulation 7920 Norfolk Avenue Bethesda, Maryland 20014 Ronald L. Bullard Chief, Environmental Specialist Branch W. Gamill Chief, Site Analysis Branch
2	Energy Research and Development Administration Division of Production & Material Management Washington, D. C. 20545 William L. Lennemann Chief, Chemical Process James W. Pollock
2	Energy Research and Development Administration Idaho Falls, Idaho 83401 Dr. Adrian H. Dahl Chief, Environmental Science Branch B. L. Schmalz

No. of Copies	Off-Site
2	U. S. Geological Survey 2100 M. Street Washington, D. C. 20037 George Debuchananne, Director M. K. Hubbert Research Geophysicist
1	U. S. Geological Survey Menlo Park, California 94025 Jacob Rubin
1	U. S. Geological Survey Groundwater Branch Denver, Colorado 80225 R. W. Stallman
1	U. S. Geological Survey Water Resources Division Bldg. 53 Federal Center Lakewood, Colorado 80225 D. Briane Adams
1	U. S. Geological Survey Water Resources Division Reston, Virginia 22092 J. D. Bredehoeft
1	U. S. Geological Survey Water Resources Division P.O. Box 917 Council Bluffs, Iowa 51501 O. J. Ramsvick Supervisory Hydrologist
1	U. S. Geological Survey Water Resources Division P.O. Box 2857 Raleigh, North Carolina 27202 Ralph C. Heath District Chief

No. of Copies	Off-Site
2	U. S. Bureau of Mines Spokane Mining Research Laboratory N. 1430 Washington St. Spokane, Washington 99201 Robert C. Bates Michael M. McDonald
1	Environmental Protection Agency Crystal Mall Washington, D. C. 20460 Arnold Joseph
1	Environmental Protection Agency Office of Research & Monitoring Edison Water Quality Office Edison, New Jersey 08817 Richard Field
1	National Water Commission 800 N. Quincy Arlington, Virginia 22209 Dr. John S. Gladwell
1	USDA-ARS Engineering Research Center CSU Foothills Campus Fort Collins, Colorado 80521 Dr. David A. Woolhiser Hydraulic Engineer
1	USDA-ARS P.O. Box 1096 Boise, Idaho 83701 J. L. Robins
1	USDA-ARS Snake River Conservation Research Center Route 1, Box 186 Kimberly, Idaho 83341 Dr. Marvin E. Jensen, Director

No. of Copies	Off-Site
1	USDA Hydrograph Laboratory Plant Industry Station Soils Building Beltsville, Maryland 20705 H. N. Holton, Director
1	USDA Sedimentation Laboratory P.O. Box 30 Oxford, Mississippi 38655 A. R. Robinson, Director
1	USDA-ARS North Central Watershed Research Center P.O. Box 916 Columbia, Missouri 65201 Dr. C. R. Amerman Hydraulic Engineer
1	USDA-ARS Northeast Watershed Research Center Pensylvania State University 111 Research Building 3 University Park, Pennsylvania 16802 Dr. A. S. Rogowski Soil Scientist
1	National Academy of Science U. S. National Committee for the IHD 2101 Constitution Avenue Washington, D. C. 20418 Dr. Leo Heindl Executive Secretary
1	National Academy of Science Committee on Radioactive Waste Management National Research Council 2101 Constitution Avenue Washington, D. C. 20418 Dr. Cyrus Klingsberg Technical Secretary

No. of Copies	Off-Site
1	National Science Foundation Division of Advanced Technology Application 1800 Sixth Street N.W. Washington, D. C. 20530 Ray Zahradnik
1	Robert S. Kerr Water Research Center P.O. Box 1198 Ada, Oklahoma 74820 Dr. J. W. Keeley
1	Alabama Geologic Survey P.O. Box Drawer 0 University, Alabama 35486 Phil Lammereaux State Geologist
1	Idaho Bureau of Mines & Geology University of Idaho Moscow, Idaho 83843 Dr. Roy E. Williams
1	Idaho Department of Water Administration State House, Annex 2 Boise, Idaho 83707 Keith R. Higginson, Director
1	Idaho Water Resources Board Boise, Idaho R. R. Lee
1	Illinois State Water Survey P.O. Box 232 Urbana, Illinois 61801 Keros Cartwright

No. of Copies	Off-Site
1	State of Maine Environmental Improvement Commission Augusta, Maine 04330 Steven D. Freedman
1	St. Anthony Falls Hydraulic Laboratory Mississippi River at Third Avenue East Minneapolis, Minnesota 55414 Professor C. Edward Bowers
1	Desert Research Institute Center for Water Resources Research Reno, Nevada Dr. Clinton Case
1	State of North Carolina Groundwater Division Water and Air Resources Raleigh, North Carolina 27611 Harry M. Peek, Chief
1	Water Quality Management Laboratory Rt. 2, Box 322A Durant, Oklahoma 74701 V. L. Hauser
1	State of Oregon 516 Public Service Bldg. Salem, Oregon 97310 Chris Wheeler State Engineer
1	State of Washington Department of Ecology Olympia, Washington 98504 Eugene F. Wallace

No. of Copies	Off-Site
1	Washington State Water Research Center Pullman, Washington 99163 James Crosby, III Geologist
1	Atomic Industrial Forum, Inc. 475 Park Avenue South New York, New York 10016 Gerald V. Halvorsen Environmental Projects Manager
1	Boeing Computer Services Federal Building Richland, Washington 99352 R. W. Nelson
1	Sandia Laboratories Division 5166 Albuquerque, New Mexico 87115
1	University of Arizona Office of Arid Lands Studies 1201 East Speedway Blvd. Tucson, Arizona 95719 Dr. Ken Faster
1	University of Arizona Department of Hydrology and Water Resources 200-E Old Psychology Tucson, Arizona 95721 Dr. A. K. Tyagi
1	University of Arizona Tucson, Arizona 95721 E. S. Simpson

No. of Copies	Off-Site
2	University of California Berkeley, California 94720 Dr. Warren Kauffman P. A. Witherspoon Department of Civil Engineering
1	University of California at Davis Department of Water Sciences and Engineering Davis, California 95616 J. N. Luthin
1	University of California at Riverside College of Biological & Agricultural Sciences Riverside, California 92507 Dr. N. T. Coleman
1	Stanford University Department of Civil Engineering Stanford, California 94305 Paul Kruger
1	Stanford University School of Earth Sciences Department of Ecology Stanford, California 94305 E. Aguado
1	Georgia Institute of Technology School of Civil Engineering Atlanta, Georgia 30332 Dr. J. R. Wallace
2	University of Illinois Urbana, Illinois 61801 A. Klute Professor Ven Te Chow Hydrosystems Laboratories

No. of Copies	Off-Site
1	Iowa State University Ames, Iowa D. Kirkham
1	Massachusetts Institute of Technology 77 Massachusetts Avenue Room 48-263 Cambridge, Massachusetts 02139 Dr. Donald Harleman
1	University of Minnesota Department of Civil Engineering Minneapolis, Minnesota 55418 H. Steforn
2	University of Nebraska School of Civil Engineering Lincoln, Nebraska 68503 Mark J. Hammer Warren Viessman, Jr.
1	Princeton University School of Engineering/Applied Science Department of Civil and Geological Engineering Princeton, New Jersey 08540 Dr. Robert W. Cleary
2	Princeton University Department of Civil and Geological Engineering Princeton, New Jersey 08540 R. J. M. DeWiest G. F. Pinder

No. of Copies	Off-Site
1	New Mexico State University Department of Agronomy P. O. Box 3Q Las Cruces, New Mexico 88001 P. J. Wierenga
1	New Mexico Institute of Mining and Technology Department of Geosciences Socorro, New Mexico 87801 Lynn W. Gelhar
1	State University of New York at Buffalo Department of Mechanical Engineering Buffalo, New York 14214 Ralph T. Cheng
1	State University of New York at Buffalo Department of Civil Engineering Buffalo, New York 14214 Dr. Ralph Rumer
1	Cornell University School of Civil Engineering B22 Bailey Hall Ithaca, New York 14850 W. H. Brutsaert
1	Oregon State University Corvallis, Oregon 97331 Dr. Larry Boersma Professor of Soils
1	Drexel Institute of Technology Philadelphia, Pennsylvania 19104 Irwin Remson
1	Vanderbilt University Nashville, Tennessee 37203 Dr. Frank L. Parker

No. of Copies	Off-Site
1	Utah State University Utah Water Research Laboratory College of Engineering Logan, Utah 84321 J. Paul Riley
1	University of Wyoming Laramie, Wyoming 92070 Dr. Paul A. Rechard Director, Water Resources Research
1	Washington State University Department of Civil Engineering 148 Sloan Hall Pullman, Washington 99163 Dr. Donald L. Bender
2	Washington State University Department of Agronomy and Soils Pullman, Washington 99163 Dr. Walter H. Gardner Dr. Gaylon S. Campbell
1	Washington State University Albrook Hydraulic Laboratory Pullman, Washington 99163 Dr. John F. Orsborn, Head
1	Washington State University Agricultural Engineering Department Pullman, Washington 99163 Dr. L. G. King
1	University of Wisconsin Department of Soil Science Madison, Wisconsin 53706 W. R. Gardner

No. of Copies	Off-Site
1	University of New South Wales School of Civil Engineering Sydney, Australia Dr. K. K. Watson
1	McMaster University Department of Civil Engineering Hamilton, Ontario, Canada Dr. William James
1	Institut de Mecanique (I.M.G.) Domaine Universitaire B. P. 53 Centre de Tri 38041 Grenoble-Cedex, France Georges Vachaud
1	Technion-Israel Institute of Technology Haifa, Israel J. Bear
1	AERE Harwell Oxfordshire, England Dr. K. L. Kipp
	On-Site Hanford
9	ERDA Richland Operations Office O. J. Elgert J. L. Rhoades P. J. Holsted (2) E. B. Jackson P. G. Rhoades R. B. Goranson B. J. Melton G. J. Bracken

No. of Copies	On-Site Hanford
30	Atlantic Richfield Hanford Co.
	R. C. Arnett (10)
	H. Babad
	D. J. Brown
	R. A. Deju
	F. R. Dornheim
	P. A. Eddy (10)
	R. E. Gephart
	R. E. Isaacson
	R. K. Ledgerwood
	M. W. Legatski
	W. H. Riggsbee
	H. P. Shaw
1	Westinghouse Hanford Co. HEDL
	R. B. Hall
53	Battelle-Northwest
	D. B. Cearlock (3)
	J. R. Eliason
	A. E. Reisenauer (20)
	R. J. Serne
	D. R. Friedrichs
	S. W. Ahlstrom
	R. G. Baca
	C. R. Cole (10)
	A. Brandstetter
	R. W. Wallace
	J. J. Fuquay
	G. W. Dawson
	Tech. Information
	Tech. Pubs.
1	United Nuclear, Inc.
	A. L. Cucchiara